NBS

Technical Note *No. 330*

Boulder Laboratories

COMPUTATIONS OF THE ANTENNA CUT-BACK FACTOR FOR LF RADIO WAVES

DUANE C. HYOVALTI

U. S. DEPARTMENT OF COMMERCE
NATIONAL BUREAU OF STANDARDS

THE NATIONAL BUREAU OF STANDARDS

The National Bureau of Standards is a principal focal point in the Federal Government for assuring maximum application of the physical and engineering sciences to the advancement of technology in industry and commerce. Its responsibilities include development and maintenance of the national standards of measurement, and the provisions of means for making measurements consistent with those standards; determination of physical constants and properties of materials; development of methods for testing materials, mechanisms, and structures, and making such tests as may be necessary, particularly for government agencies; cooperation in the establishment of standard practices for incorporation in codes and specifications; advisory service to government agencies on scientific and technical problems; invention and development of devices to serve special needs of the Government; assistance to industry, business, and consumers in the development and acceptance of commercial standards and simplified trade practice recommendations; administration of programs in cooperation with United States business groups and standards organizations for the development of international standards of practice; and maintenance of a clearinghouse for the collection and dissemination of scientific, technical, and engineering information. The scope of the Bureau's activities is suggested in the following listing of its four Institutes and their organizational units.

Institute for Basic Standards. Applied Mathematics. Electricity. Metrology. Mechanics. Heat. Atomic Physics. Physical Chemistry. Laboratory Astrophysics.* Radiation Physics. Radio Standards Laboratory:* Radio Standards Physics; Radio Standards Engineering. Office of Standard Reference Data.

Institute for Materials Research. Analytical Chemistry. Polymers. Metallurgy. Inorganic Materials. Reactor Radiations. Cryogenics.* Materials Evaluation Laboratory. Office of Standard Reference Materials.

Institute for Applied Technology. Building Research. Information Technology. Performance Test Development. Electronic Instrumentation. Textile and Apparel Technology Center. Technical Analysis. Office of Weights and Measures. Office of Engineering Standards. Office of Invention and Innovation. Office of Technical Resources. Clearinghouse for Federal Scientific and Technical Information.**

Central Radio Propagation Laboratory.* Ionospheric Telecommunications. Tropospheric Telecommunications. Space Environment Forecasting. Aeronomy.

---

* Located at Boulder, Colorado 80301.
** Located at 5285 Port Royal Road, Springfield, Virginia 22171.

NATIONAL BUREAU OF STANDARDS

Technical Note. 330

ISSUED November 26, 1965

COMPUTATIONS OF THE ANTENNA CUT-BACK FACTOR FOR LF RADIO WAVES

Duane C. Hyovalti
Institute for Telecommunication Sciences and Aeronomy[*]
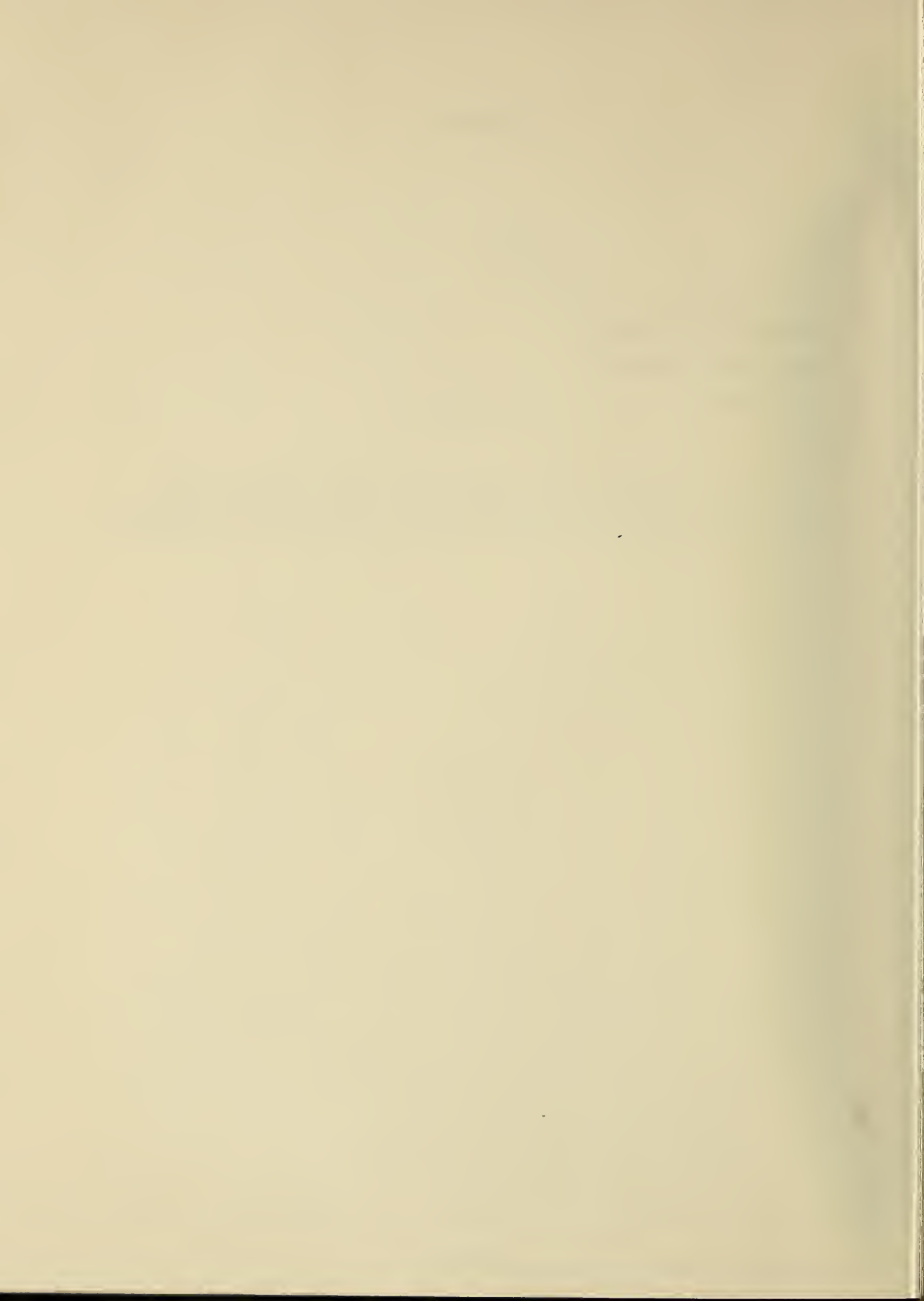Environmental Science Services Administration

NBS Technical Notes are designed to supplement the Bureau's regular publications program. They provide a means for making available scientific data that are of transient or limited interest. Technical Notes may be listed or referred to in the open literature.

Foreword

Contents

Computations of the Antenna Cut-Back Factor for LF Radio Waves

Duane C. Hyovalti

There are several methods for evaluating the cut-back factor of geometric optics, e. g., the flat-earth approximation, the contour integral, and the residue series summation methods. Wait and Conda give quite extensive details of the theory of these three methods in their 1958 paper, and Johler [1961, 1962] elaborates even further. In this paper each of the above mentioned methods is investigated, and calculations are made for various frequencies and distances. The frequencies used are primarily LF; however, frequencies up to 1 Mc/s are considered. Several conductivities and dielectric constants are used, varying from sea water ($\sigma = 5$ mhos/m, $\epsilon_2 = 80$) to typical earth ($\sigma = 0.005$ mhos/m, $\epsilon_2 = 15$). The permittivity lapse factor, α, is varied from 0.75 to 1.0 with most of the computations being done for $\alpha = 0.75$ and 0.85. Only calculations for vertical electric polarization were carried out in this paper.

Key Words: antenna cut-back factor, computations, low frequency radio waves, geometric optics, flat-earth approximation.

1. Introduction

The propagation of a low-frequency (LF) radio signal is represented pictorially by figure 1. The LF wave is transmitted from one point on the earth to another point, i. e., from S to O where S is the source and O is the observer (figure 1). The distance in meters from S to O along the surface of the spherical earth is d, the radius of the earth in meters is a, h is the height of the ionosphere in meters, and θ, the angle at the center of the earth subtended by the distance d, is defined as follows:

$$d = a\,\theta. \tag{1}$$

In geometric-optical theory [Bremmer, 1949], the LF wave travels by a ray path from the transmitter to the receiver either along the surface of the earth, known as the ground wave, or by being reflected from the ionosphere, known as the sky wave. The total field, $E(\omega, d)$, which depends upon the frequency $f = \omega/2\pi$, cycles/second, and the distance d, is defined [Johler, 1961] by

$$E(\omega, d) = \sum_{j=0}^{P} E_j(\omega, d), \qquad (2)$$

where $E_0(\omega, d)$ is the ground wave and $E_j(\omega, d)$, $j \neq 0$, corresponds to the waves reflected by the ionosphere and is

$$E_j(\omega, d) = i\omega d \, D_j^{-1} C \exp(i\omega t_j') G_j^t G_j^r \alpha_j F_j C_j, \qquad (3)$$

where D_j is the physical length of the geometric-optical ray and C is a function of distance, $C = 10^{-7}/d$, for a dipole source current moment $I_0 \ell = 1$. The local sky wave time is t_j', the G's are the antenna pattern factors, α_j is the classical convergence-divergence coefficient modified by a convergence correction [Wait, 1960], F_j is the cut-back factor [Wait and Conda, 1958], and C_j is the effective reflection coefficient composed of the Fresnel ground reflection coefficients and ionospheric reflection coefficients (see Johler [1961, 1962]). The subject of this paper will be the cut-back factor F_j. However, before going into any detail about F_j, several of the remaining parameters shown in figure 1 will be defined.

2.   Mathematical Theory

The angle of incidence of the ray on the ionosphere, $\varphi_{i,j}$, and the corresponding angle of incidence on the earth, τ_j, where j refers to a particular ionospheric wave or hop, can easily be evaluated from the geometry of figure 1. If

$$\Delta_j = \left[2a(a+h)\left(1 - \cos\frac{\theta}{2j}\right) + h^2 \right]^{\frac{1}{2}}, \qquad (4)$$

then

$$\sin \tau_j = \Delta_j^{-1} (a + h) \sin \frac{\theta}{2j}, \tag{5a}$$

$$\cos \tau_j = \Delta_j^{-1} \left[a \left(\cos \frac{\theta}{2j} - 1 \right) + h \cos \frac{\theta}{2j} \right]. \tag{5b}$$

The wave number of the air, k_1, and the wave number of the ground, k_2, are defined as follows:

$$k_1 = \frac{\omega}{c} \eta_1, \tag{6}$$

$$k_2 = \frac{\omega}{c} \left[\epsilon_2 - i \frac{\sigma \mu_0 c^2}{\omega} \right]^{\frac{1}{2}}, \tag{7}$$

where η_1 is the index of refraction of air (1. 000338), c is the velocity of light ($\sim 3(10^8)$ m/sec), ϵ_2 is the dielectric constant of the earth, σ is the conductivity of the earth in mhos/m, and μ_0 is the permeability ($4\pi (10^{-7})$ h/m). For typical land, $\epsilon_2 = 15$ and $\sigma = 0.005$ mhos/m, whereas for sea water, $\epsilon_2 = 80$ and $\sigma = 5$ mhos/m. As the geometric-optical horizon is approached, $\tau_j \sim \frac{\pi}{2}$ which is represented for j = 1 by the dotted lines in figure 1.

The cut-back factor F_j, where $F_j = F_j^t F_j^r$, takes account of the diffraction of rays by the earth's curvature. If it is assumed that the geometric-optical ray is not too close to or beyond the geometric-optical horizon, then the flat-earth approximation to the cut-back factor composed of the Fresnel ground reflection coefficients, R_e and R_m, satisfies all the requirements of determining F_j^t and F_j^r. For vertical polarization

$$F_j^{t,r} \sim [1 + R_e^{t,r}(\tau_j)], \tag{8}$$

where the subscript e refers to vertical electric polarization and the superscripts t and r refer to the transmitter and receiver, respectively. The factor $F_j^{t,r}$ is similarly determined for horizontal polarization by using R_m. The Fresnel ground reflection coefficients are

$$R_e(\tau_s) = \frac{\left(\dfrac{k_2}{k_1}\right)^2 \cos \tau_s - \left[\left(\dfrac{k_2}{k_1}\right)^2 - \sin^2 \tau_s\right]^{\frac{1}{2}}}{\left(\dfrac{k_2}{k_1}\right)^2 \cos \tau_s + \left[\left(\dfrac{k_2}{k_1}\right)^2 - \sin^2 \tau_s\right]^{\frac{1}{2}}} \tag{9}$$

for vertical polarization and

$$R_m(\tau_s) = \frac{\cos \tau_s - \left[\left(\dfrac{k_2}{k_1}\right)^2 - \sin^2 \tau_s\right]^{\frac{1}{2}}}{\cos \tau_s + \left[\left(\dfrac{k_2}{k_1}\right)^2 - \sin^2 \tau_s\right]^{\frac{1}{2}}} \tag{10}$$

for horizontal polarization.

   If the geometric-optical ray is close to or beyond the geometric-optical horizon, then the contour integral for $F_1^{t,r}$ introduced and developed by Wait and Conda [1958] and used extensively by Johler [1961, 1962] can be evaluated by using a Gaussian quadrature to integrate numerically. The factor $F_1^{t,r}$ in contour integral form is

$$F_1^{t,r} \sim (\pi)^{-\frac{1}{2}} \exp(-ik_1 a\theta') \int_{\infty \, \exp(-i 2\pi/3)}^{\infty} \frac{\exp\left[-i(k_1 a/2)^{\frac{1}{3}} \theta' \rho\right]}{W_1'(\rho) - q W_1(\rho)} d\rho, \tag{11}$$

where $\theta' = (d - d_H)/2a$ and d_H is the distance from the transmitter to the geometric-optical horizon. An effective earth radius a_e is used in place of the actual earth's radius, a, such that $\dfrac{a}{a_e} = \alpha$ where α is the vertical lapse of the permittivity of air at the earth's surface and usually varies from 0.75 to 0.85. The functions $W_1(\rho)$ and $W_1'(\rho)$ are defined by Fock [1946] and used extensively by Wait and Conda [1958]. These functions are closely related to Airy integrals and Hankel functions of orders $\frac{1}{3}$ and $\frac{2}{3}$ (see Wait and Conda [1958]; Johler [1961, 1962]) and are given as follows:

$$W_1(\rho) = \exp\left[-i2\pi/3\right] \sqrt{\frac{\pi}{3}} \, (-\rho)^{\frac{1}{2}} H_{\frac{1}{3}}^{(2)} \left[\frac{2}{3}(-\rho)^{\frac{3}{2}}\right], \qquad (12)$$

and

$$W_1'(\rho) = \exp\left[-i4\pi/3\right] \sqrt{\frac{\pi}{3}} \, \rho \, H_{\frac{2}{3}}^{(2)} \left[\frac{2}{3}(-\rho)^{\frac{3}{2}}\right], \qquad (13)$$

where $H_{\frac{1}{3}}^{(2)}(z)$ and $H_{\frac{2}{3}}^{(2)}(z)$ are Hankel functions of the second kind and of orders $\frac{1}{3}$ and $\frac{2}{3}$, respectively. The arg ρ has the following restrictions:

$$-\frac{\pi}{3} \le \arg \rho < \frac{5\pi}{3},$$

and

$$\arg(-\rho) = \arg \rho - \pi$$

$$\arg \rho^{m/n} = \frac{m}{n} \arg \rho \text{ where m and n are integers.}$$

The factor q is defined

$$q = -i \left(\frac{k_1 a}{2}\right)^{\frac{1}{3}} \frac{k_1}{k_2} \sqrt{1 - \left(\frac{k_1}{k_2}\right)^2}. \qquad (14)$$

The contour integral can be written [Johler, 1962]

$$F_1^{t,r} \sim (\pi)^{-\frac{1}{2}} \exp(-ik_1 a \, \theta')$$

$$\left\{\int_0^\infty \frac{\exp\left[-i(k_1 a/2)^{\frac{1}{3}} \theta' \alpha\right]}{W_1'(\alpha) - q W_1(\alpha)} \, d\alpha - \int_0^\infty \frac{\exp\left[-i(k_1 a/2)^{\frac{1}{3}} \theta' \alpha' - i2\pi/3\right]}{W_1'(\alpha') - q W_1(\alpha')} \, d\alpha\right\} \qquad (15)$$

where $\alpha' = \alpha \exp(-i2\pi/3)$. These integrals can then be evaluated with a Gaussian quadrature. It should be noted that the right hand side of (11) exactly equals the right hand side of (15). The Airy integrals can now be evaluated using the following equations:

$$W_1(\alpha) = -i \exp\left[-i\,2\pi/3\right] \sqrt{\frac{\pi}{3}} \, \alpha^{\frac{1}{2}} \, H^{(2)}_{\frac{1}{3}}\left[\frac{2}{3} \exp(-i\,3\pi/2) \, \alpha^{\frac{3}{2}}\right] \qquad (16)$$

$$W_1'(\alpha) = \exp\left[-i\,4\pi/3\right] \sqrt{\frac{\pi}{3}} \, \alpha \, H^{(2)}_{\frac{2}{3}}\left[\frac{2}{3} \exp(-i\,3\pi/2) \, \alpha^{\frac{3}{2}}\right] \qquad (17)$$

$$W_1(\alpha') = -i \sqrt{\frac{\pi}{3}} \, \alpha^{\frac{1}{2}} \, H^{(2)}_{\frac{1}{3}}\left[\frac{2}{3} i\alpha^{\frac{3}{2}}\right] \qquad (18)$$

$$W_1'(\alpha') = \sqrt{\frac{\pi}{3}} \, \alpha \, H^{(2)}_{\frac{2}{3}}\left[\frac{2}{3} i\alpha^{\frac{3}{2}}\right], \qquad (19)$$

where α is a real positive number and the square roots involved are positive. The Hankel functions can be evaluated using the method described by Berry [1964].

Beyond and not too close to the geometric-optical horizon, the cut-back factor can be evaluated by a residue series summation [Wait and Conda, 1958; Johler, 1961, 1962]

$$F_1^{t,r} \sim -2i \sqrt{\pi} \exp(-i\,k_1 a \, \theta') \sum_{s=0}^{\infty} \frac{\exp\left[-i(k_1 a)^{\frac{1}{3}} \theta' \tau_s\right]}{(2^{\frac{1}{3}} \tau_s - q^2) \, W_1(2^{\frac{1}{3}} \tau_s)} \qquad (20)$$

where $\tau = \tau_s$ are the special roots of Riccati's differential equation noted by Bremmer [1949]

$$\frac{d\delta}{d\tau} - 2\delta^2 \tau + 1 = 0. \qquad (21)$$

The factor, δ, for vertical polarization $\delta = \delta_e$, is

$$\delta_e = \frac{-i\alpha^{\frac{1}{3}}\left(\frac{k_2}{k_1}\right)^2}{(k_1 a)^{\frac{1}{3}}\left[\left(\frac{k_2}{k_1}\right)^2 - 1\right]^{\frac{1}{2}}}. \tag{22}$$

The phase factor Δ as used by Wait and Conda [1958] is

$$\Delta = \arg F_j^{t,r} + k_1 a\,\theta' - \frac{k_1 a}{6}\,\theta'^3 \quad \text{for } \theta' < 0 \tag{23}$$

(that is for $d < d_H$) and

$$\Delta = \arg F_j^{t,r} + k_1 a\,\theta' \quad \text{for } \theta' > 0 \tag{24}$$

(that is for $d > d_H$). Thus for $\theta' < 0$, Δ is the phase difference between the incident field and the resultant field. For $\theta' > 0$, Δ is the phase difference between the electrical arc length $k_1 a\,\theta'$ and the resultant field in the shadow region [Wait and Conda, 1958]. This phase, Δ, changes much less rapidly than the phase actually calculated from (15) and (20), and is easier to represent in a graph.

3. Discussion of Figures

Figures 2 through 5 represent the amplitude and phase of the cutback factor evaluated by using the flat-earth approximation (8). These figures are given as a function of distance and are parametric in frequency. A ground conductivity of 0.005 mhos/m and a dielectric constant of 15 are assumed to obtain the amplitude and phase of $F_j^{t,r}$ shown in figures 2 and 3, respectively. These two figures are representative of the typical earth case. The amplitude and phase in figures 4 and 5 are for sea water, $\sigma = 5$ mhos/m and $\epsilon_2 = 80$. Note that the amplitude for typical earth decreases more rapidly than that for sea water as the geometric-optical horizon is approached. The same phenomenon holds true for the phase. This phase is the phase Δ since

an exponential term, $\exp[-ik_1 a \sin \theta']$, is omitted from (8), and since (23) is merely the series representation of this omitted exponential term.

The amplitude and phase curves shown in figures 6 through 23 are obtained by evaluating the integrals of (15) for various conductivities as a function of distance parametric in frequency. Figures 6 through 19 are for a permittivity lapse factor, α, of 0.75, and figures 20 through 23 are for an α of 0.85. A conductivity of 0.005 mhos/m and $\varepsilon_2 = 15$ are used to obtain the amplitude and phase curves shown in figures 6 and 7. Figures 8 through 11 give the amplitude and phase for $\sigma = 0.05$ mhos/m. An enlarged graph of the magnitude of $F_1^{t',r}$ in the region where $d \leq d_H$, shown in figure 9, reveals that the magnitude of 20 kc/s is greater than those of 50 or 100 kc/s at the geometric-optical horizon, but that it crosses over to become less than these at shorter distances. A similar enlargement of the same area for the argument of $F_1^{t',r}$, figure 11, shows no such crossover. However, maxima for the arguments of 20 and 50 kc/s will be noticed. A conductivity of 0.5 mhos/m is assumed to obtain the amplitude and phase curves in figures 12 through 15. Figures 13 and 15 show enlarged regions for $d \leq d_H$ for amplitude and phase, respectively. The amplitude of 20 kc/s crosses over all the others, 50 kc/s crosses over all the others except 20 and 1000 kc/s, etc. as shown in figure 13. All the phase curves except 500 and 1000 kc/s have maxima for $d < d_H$. For the sea water case, $\sigma = 5$ mhos/m and $\varepsilon_2 = 80$, the amplitude and phase are shown in figures 16 through 19. Close-ups of the area where $d \leq d_H$ are given again for the amplitude and phase in figures 17 and 19, respectively. In this case it is observed that all the amplitude curves cross over and that even some of the phase curves cross over in addition to having maxima in this region. It should be noted that the amplitude and phase curves decrease more rapidly for the lower conductivities than for the higher ones. Figures 20 through 23 show the magnitude and argument of $F_1^{t',r}$ for the sea water case, $\sigma = 5$ mhos/m and $\varepsilon_2 = 80$, for an α of 0.85. The same effects as are observed for the sea water case for $\alpha = 0.75$ are observed for 0.85. However, the amplitude and phase curves for $\alpha = 0.85$ tend to decrease more rapidly than those for $\alpha = 0.75$.

Figures 24 and 25 illustrate the use of the residue series summation (20), to calculate the amplitude and phase of the cut-back factor beyond the geometric-optical horizon. A conductivity of 0.005 mhos/m and $\varepsilon_2 = 15$ are used in addition to assuming $\alpha = 0.75$. If the integral method (15), and the residue series method (20), are compared, it will be seen that they fall exactly on top of one another as can be noted by comparison of figures 6 and 24, and 7 and 25. There seems to be a loss of precision in calculating the residue series method at 200 kc/s. Therefore, the integral method is used when it seems necessary.

The amplitude and phase curves shown in figures 26 through 28 are for three different sets of conditions as a function of frequency. The integral method was used to calculate the amplitude and phase curves for these three figures. Models 1 and 3 are for a height, h, of 65 km. A conductivity of 5 mhos/m and $\epsilon_2 = 80$ are used for model 1 along with a distance of 1609 km (1000 miles). A distance of 2127 km, $\sigma = 0.005$ mhos/m and $\epsilon_2 = 15$ are used for model 3. Model 2 uses a height of 45 km, a distance of 1416 km (880 miles), a conductivity of 5 mhos/m and $\epsilon_2 = 80$. All three models use an α of 0.85. The amplitudes for models 1 and 2 tend to remain almost constant or rise as the frequency increases, whereas the amplitude for model 3 decreases as the frequency increases as can be seen in figure 26. This phenomenon is primarily due to the fact that the distance for model 3 puts it well beyond the geometric-optical horizon while the distances for models 1 and 2 are less than the distance to the horizon. The fact that model 3 is a typical earth case whereas models 1 and 2 are sea water cases has some effect but much less than that caused by the distances. Figure 27 shows that the phases for models 1 and 2 reach maxima and then decrease as a function of frequency. The phase for model 3 decreases steadily as the frequency increases, as is shown in figures 27 and 28. The reason that the phase for model 3 has no maximum like those for models 1 and 2 is primarily due to the fact that model 3 is the typical earth case while models 1 and 2 are sea water cases.

Figures 29 through 32 show the amplitude and phase of the cut-back factor as a function of frequency parametric in distance. A height of 40 km, a permittivity lapse factor of 1, a conductivity of 0.005 mhos/m and $\epsilon_2 = 15$ are used for these figures. The integral method is used to obtain figures 29 and 30 while the flat-earth approximation is used to obtain figures 31 and 32. It should be noted that both the amplitude and phase obtained with the integral method reach maxima and then decrease as a function of frequency whereas they just decrease steadily for the flat-earth method.

All of the figures discussed above, figures 2 through 32, are for vertical electric polarization. It is interesting to note that the integral method works far beyond the geometric-optical horizon.

4. References

Berry, L. A. (1964), Computation of Hankel functions, NBS Tech. Note No. 216.

Bremmer, H. (1949), Terrestrial radio waves--theory of propagation (Elsevier Publishing Co., New York, N. Y.).

Fock, V. A. (1946), Diffraction of radio waves around the earth's surface (Publishers of the Academy of Science, Moscow, USSR).

Johler, J. R. (1961), On the analysis of LF ionospheric radio propagation phenomena, J. Res. NBS 65D (Radio Prop.), No. 5, 507-529.

Johler, J. R. (1962), Propagation of the low-frequency radio signal, Proc. IRE 50, No. 4, 404-427.

Wait, J. R. (1960), Diffractive corrections to the geometrical optics of low frequency propagation, Electromagnetic Wave Propagation, 87-101 (Academic Press, London, England).

Wait, J. R., and A. M. Conda (1958), Pattern of an antenna on a curved lossy surface, IRE Trans. Ant. Prop. AP-6, No. 4, 348-359.
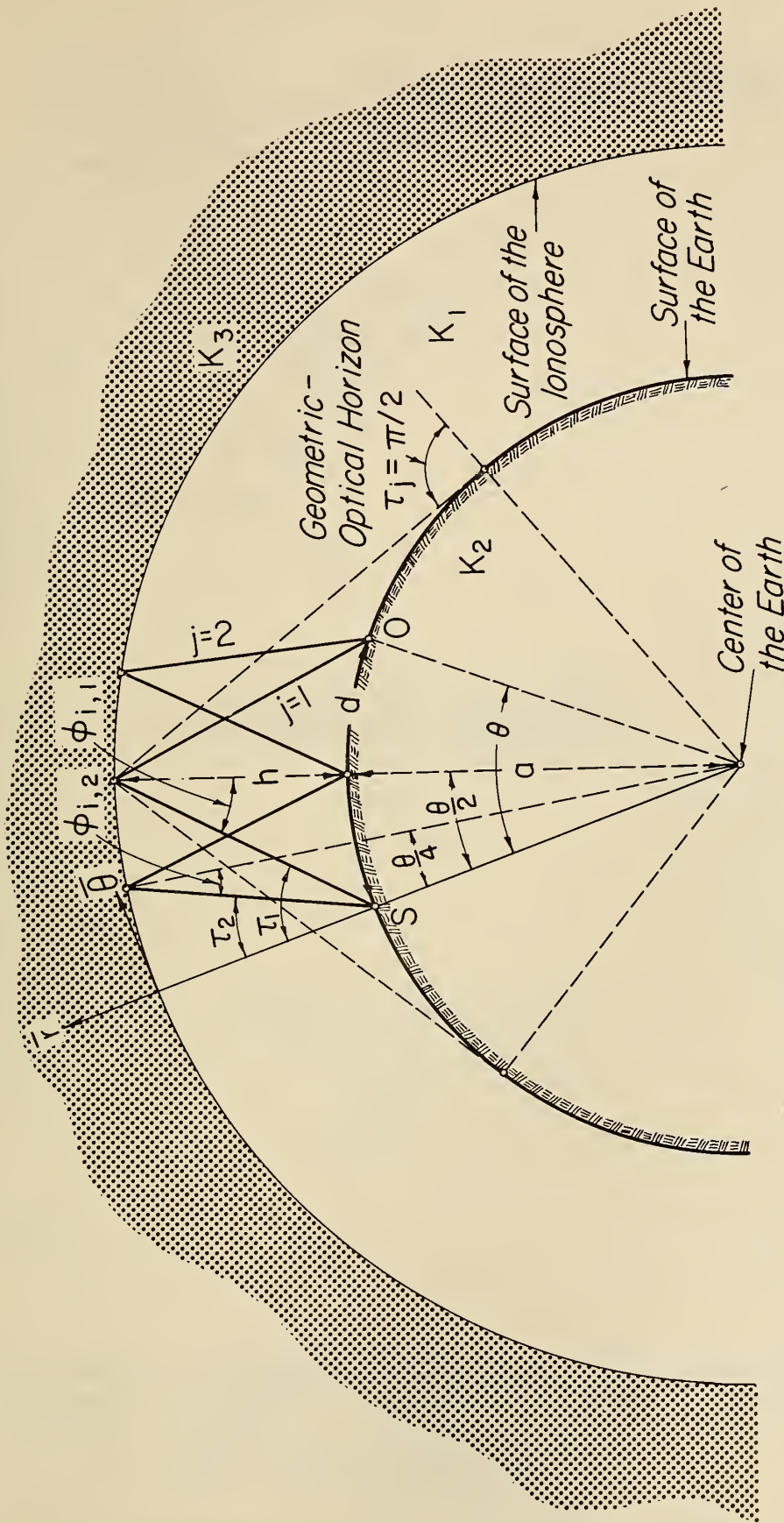
Figure 1. Propagation of low-frequency radio signals in the vicinity of the earth by geometric-optical theory.
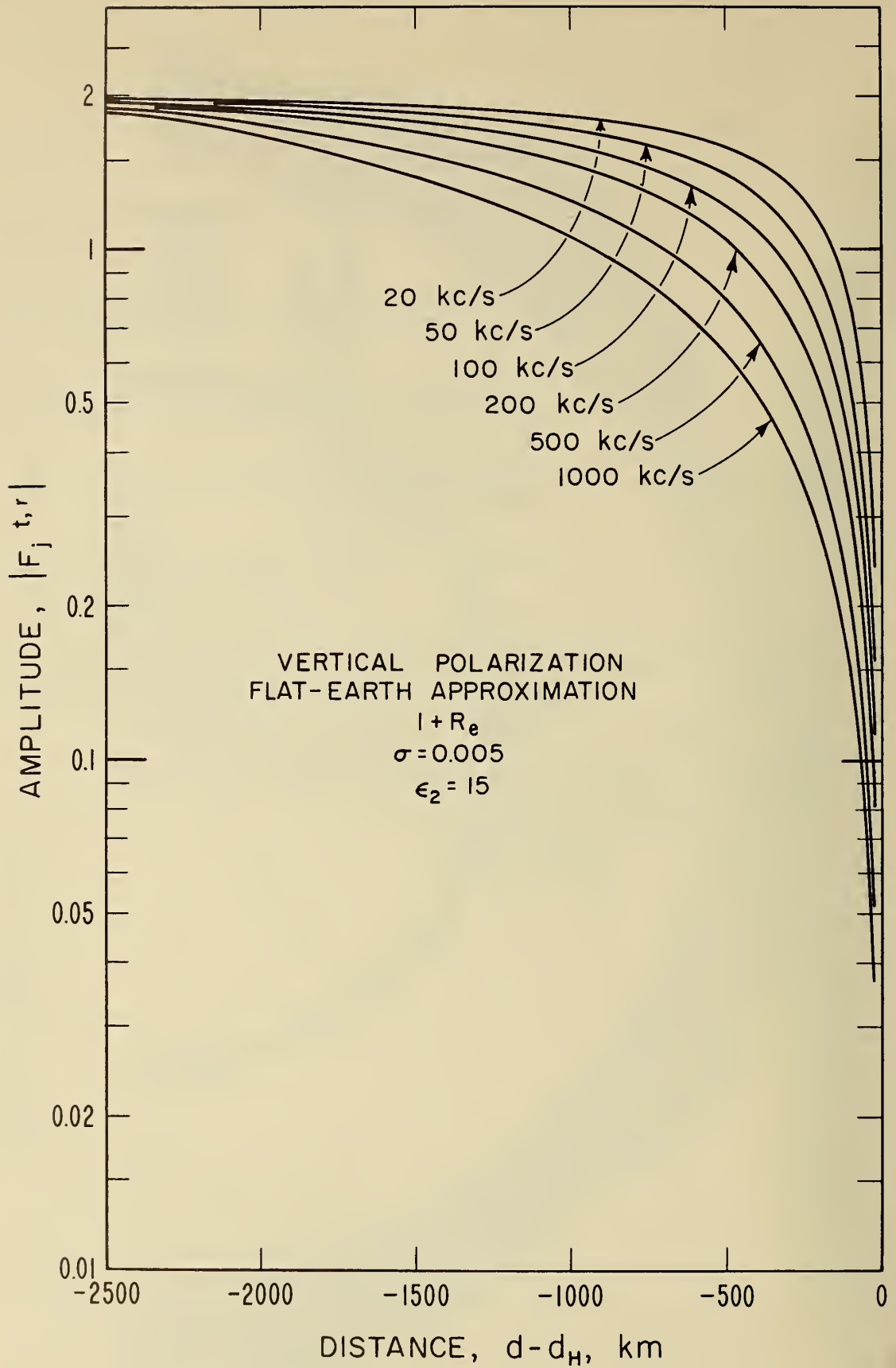
Figure 2. Amplitude of the cut-back factor $F_j^{t,r}$.
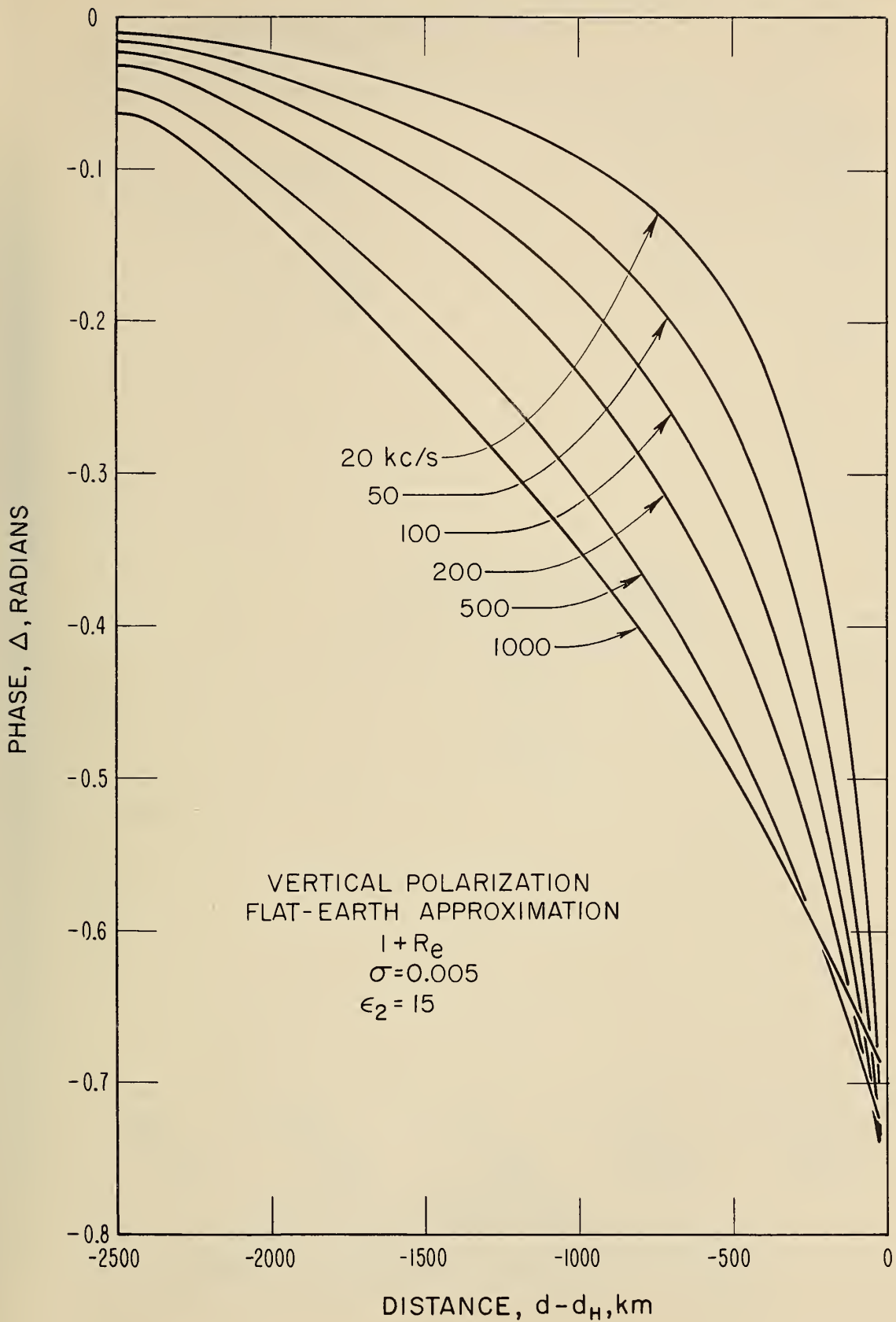
Figure 3.   Phase of the cut-back factor $F_j^{t,\,r}$.
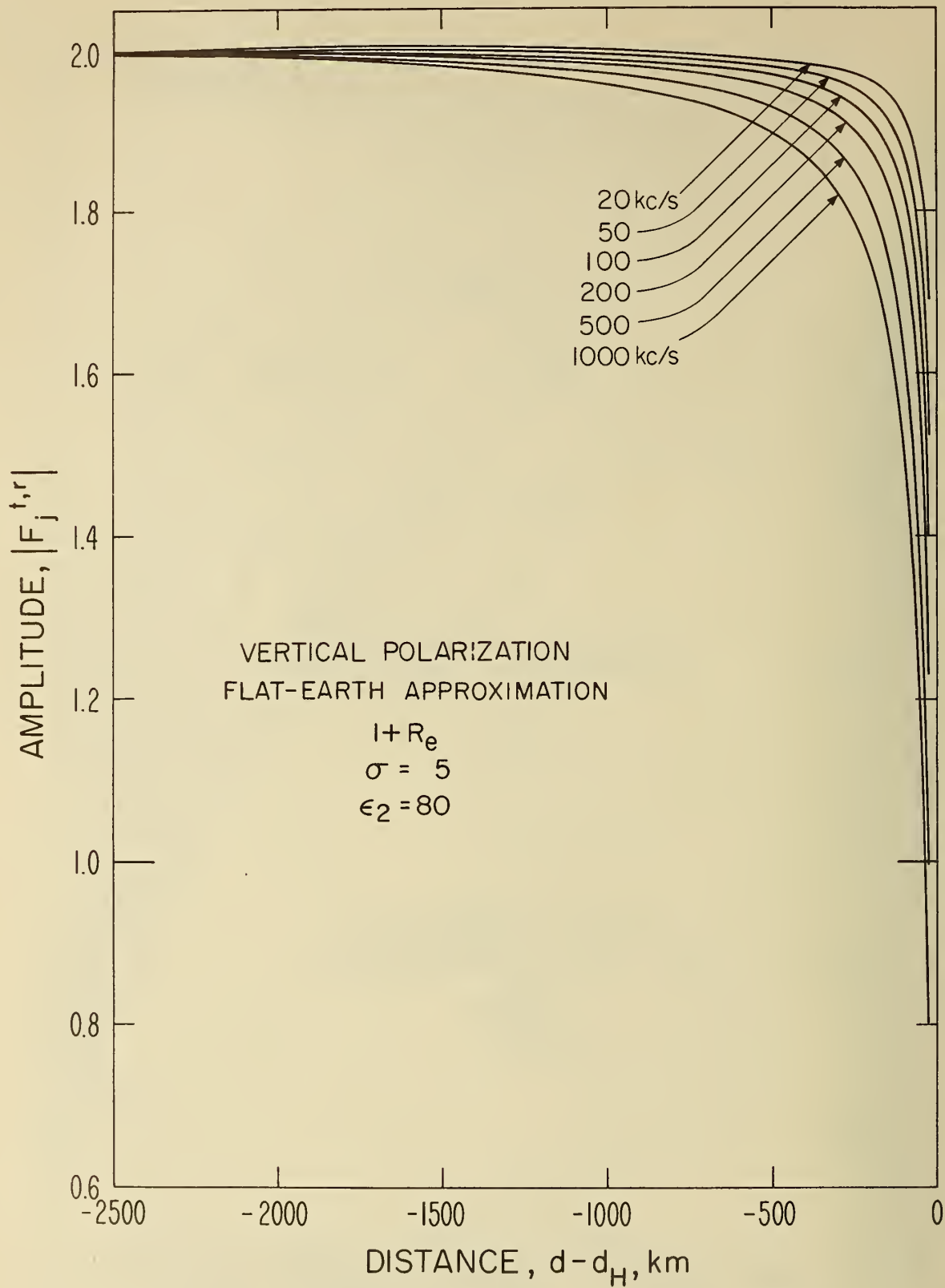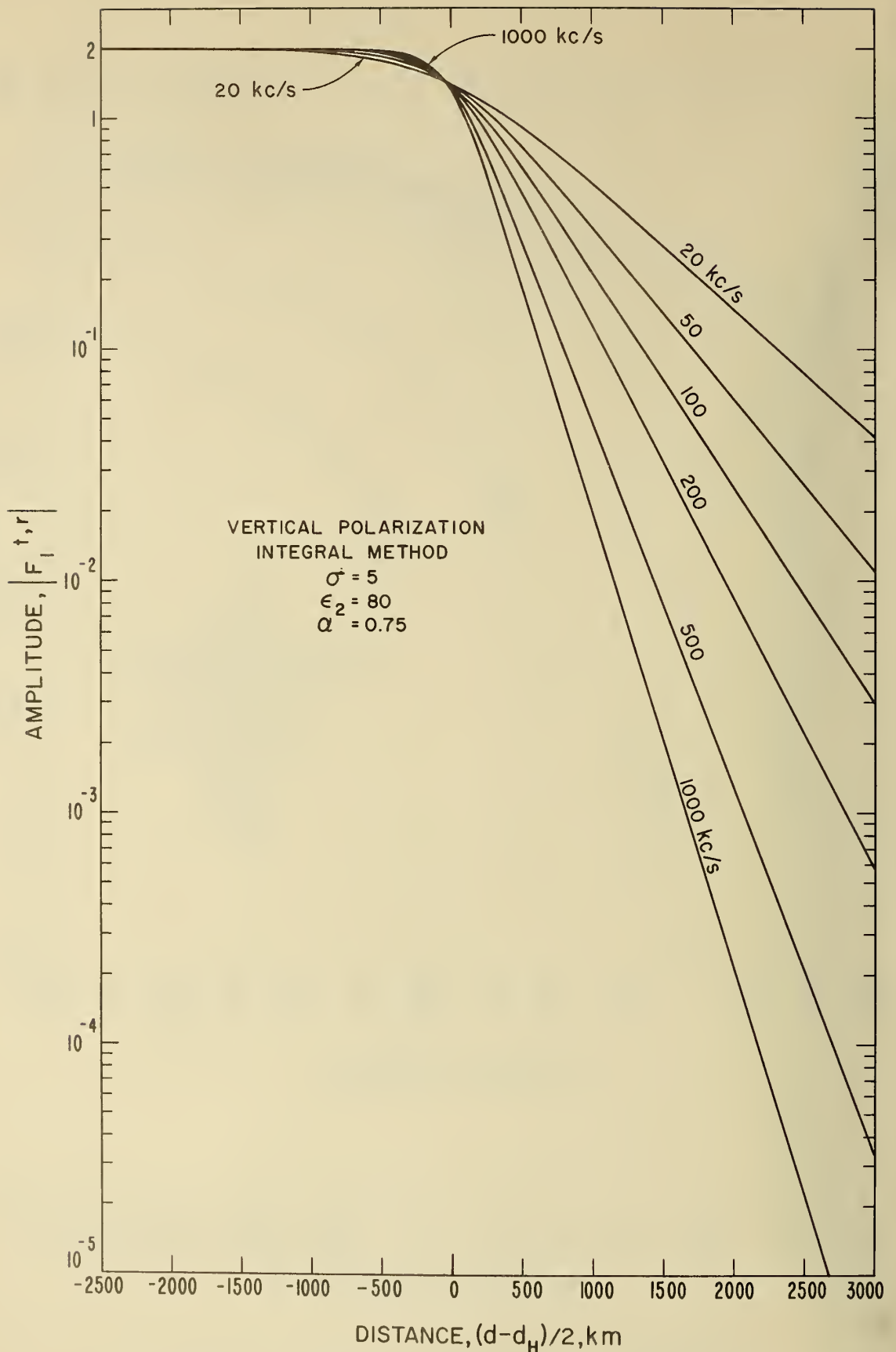
Figure 4. Amplitude of the cut-back factor $F_j^{t,r}$.
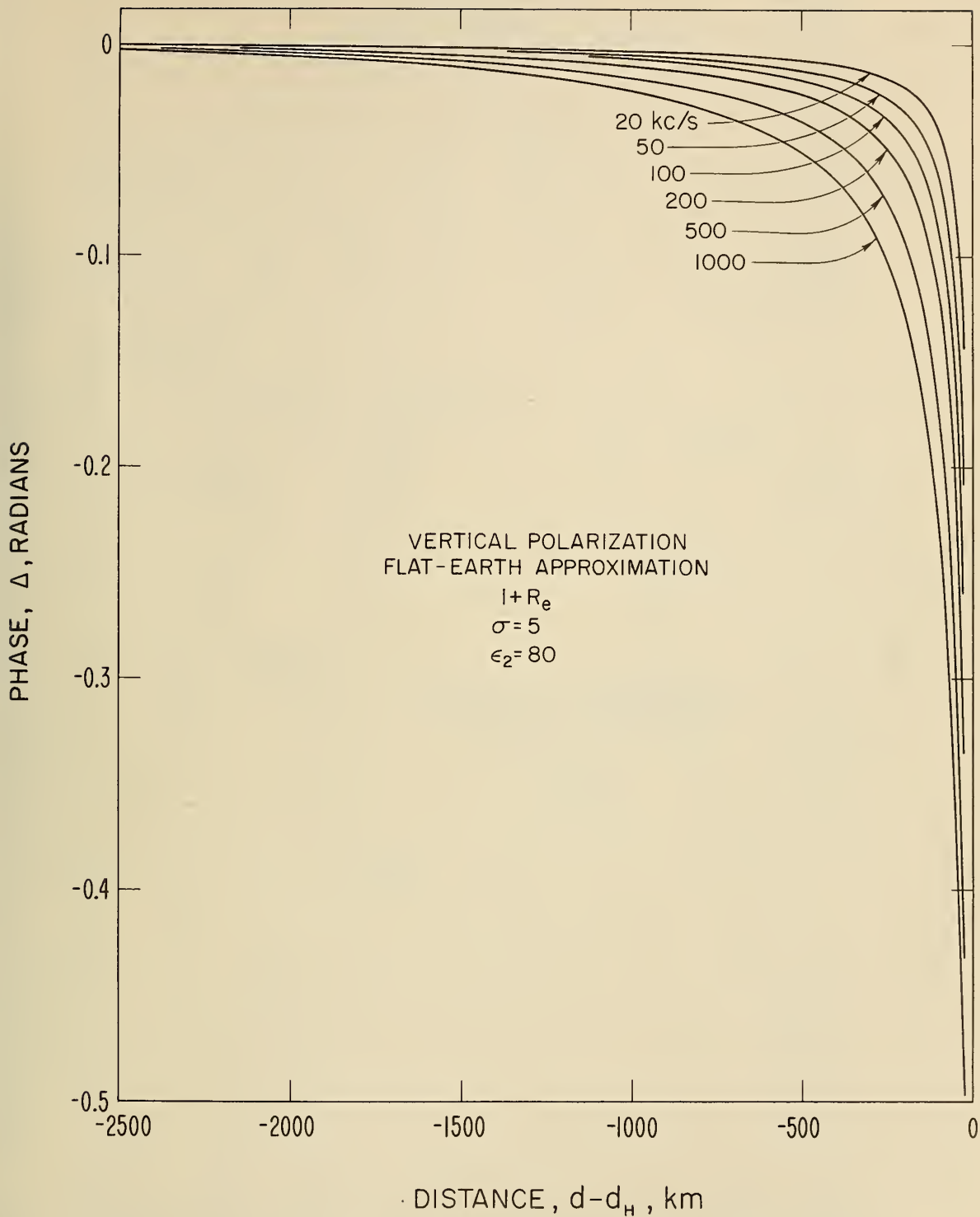
Figure 5.   Phase of the cut-back factor $F_j^{t, r}$.
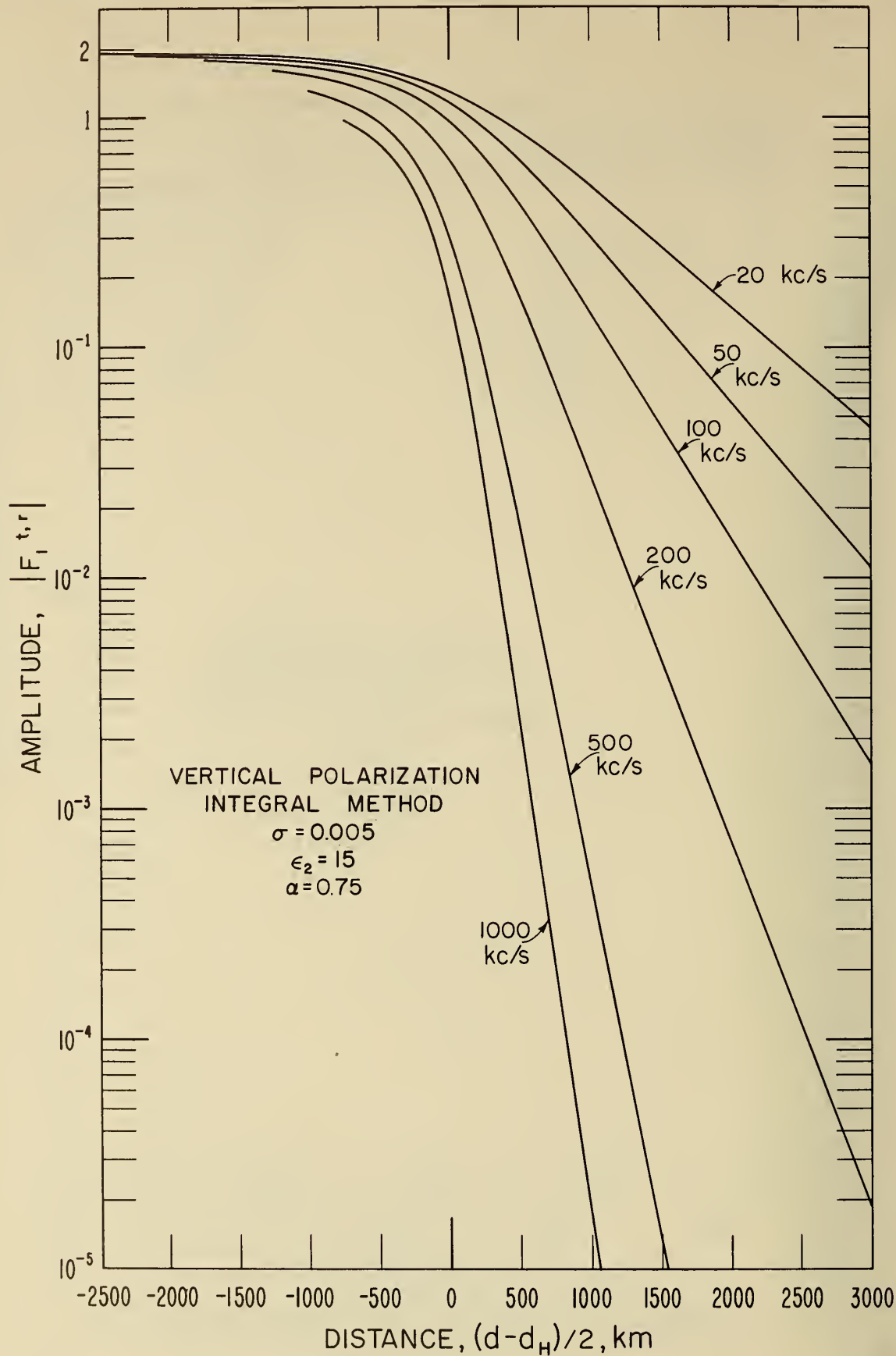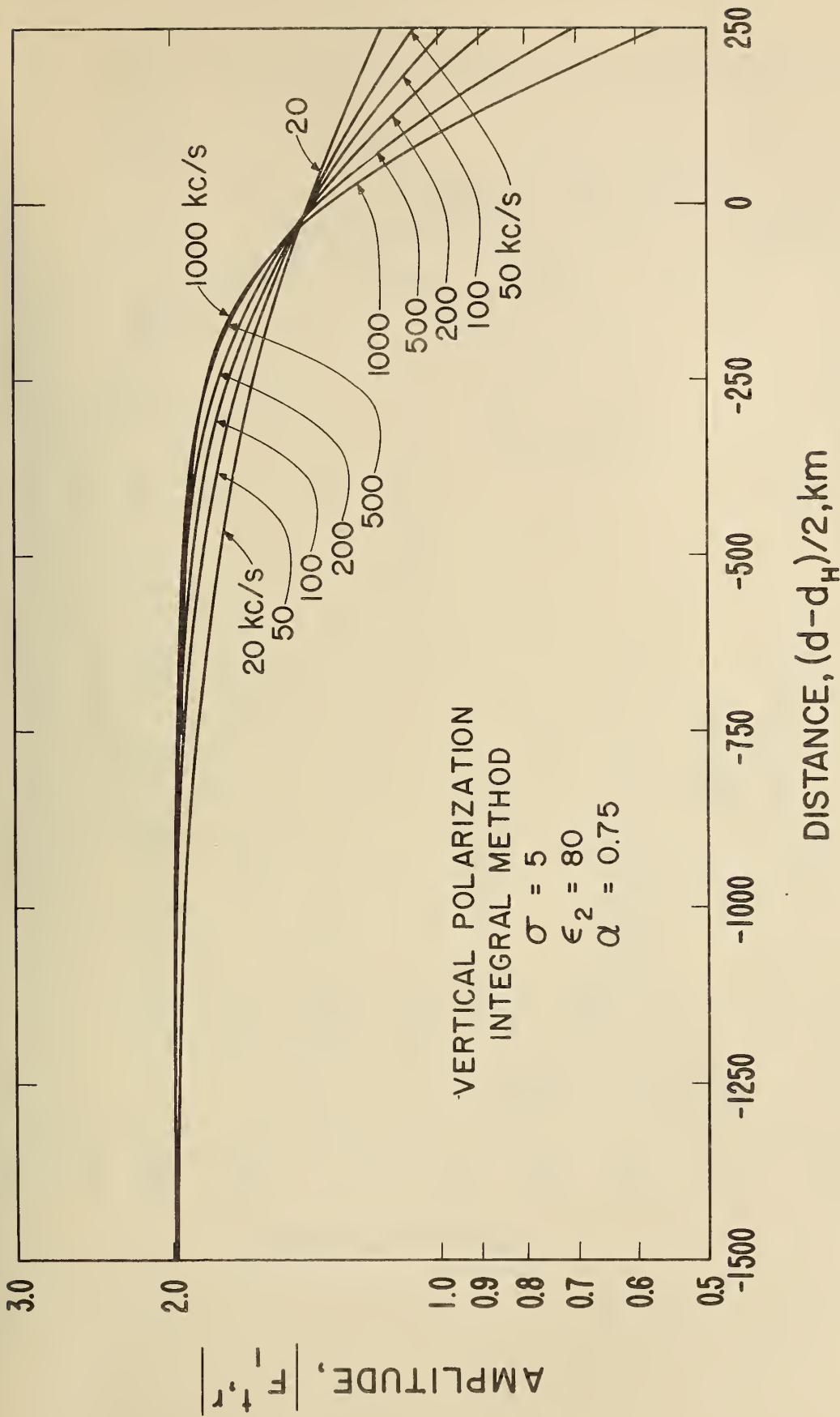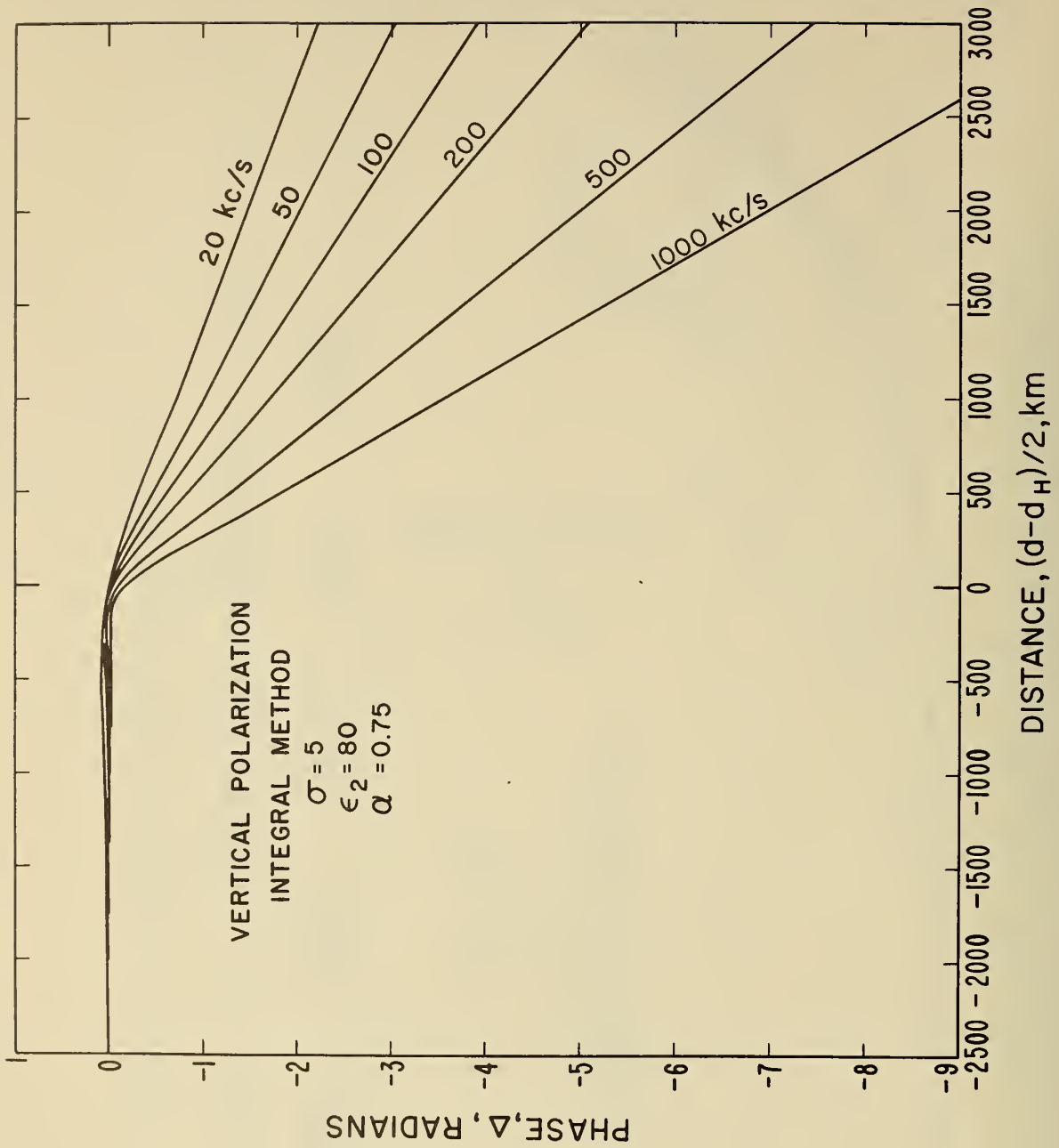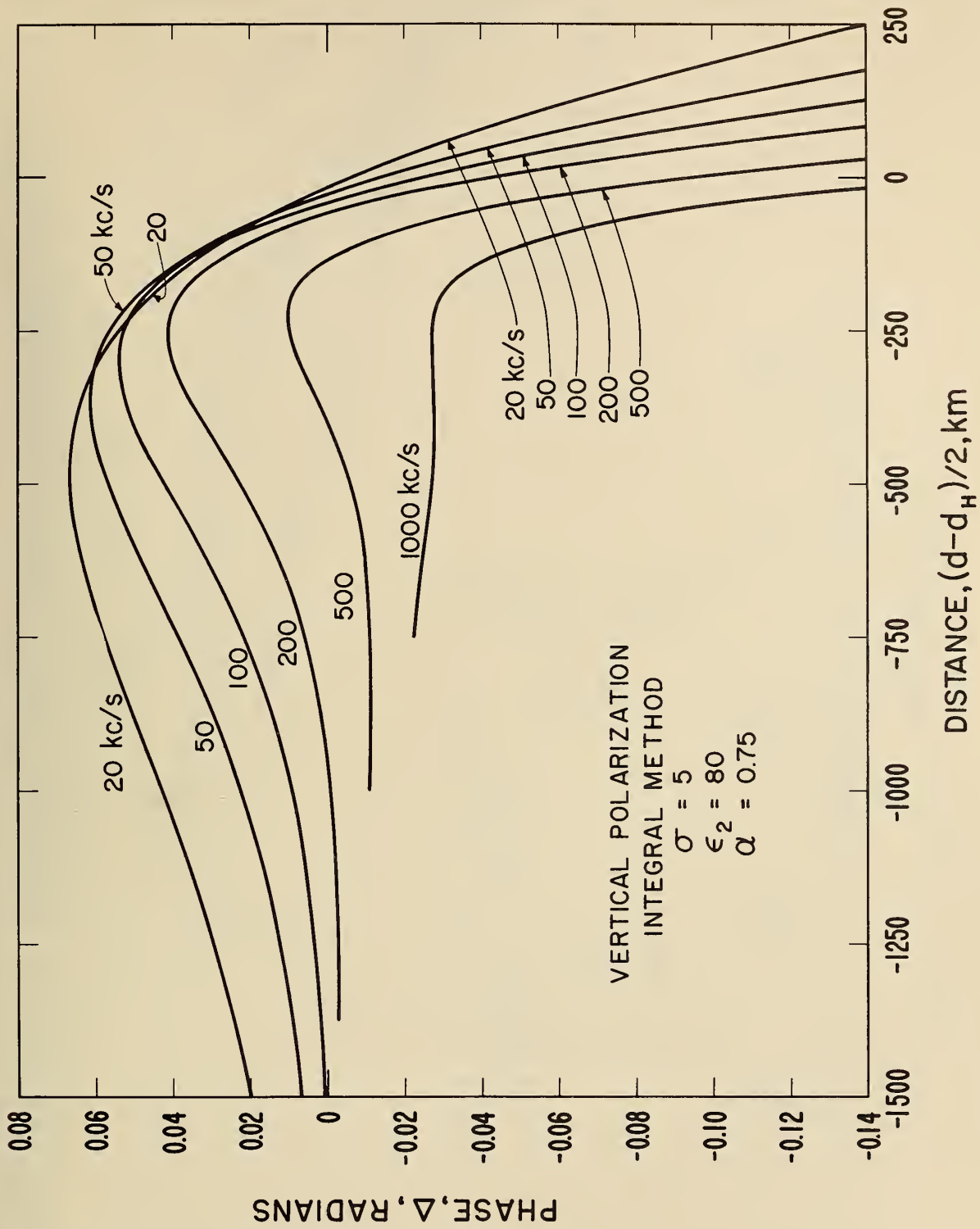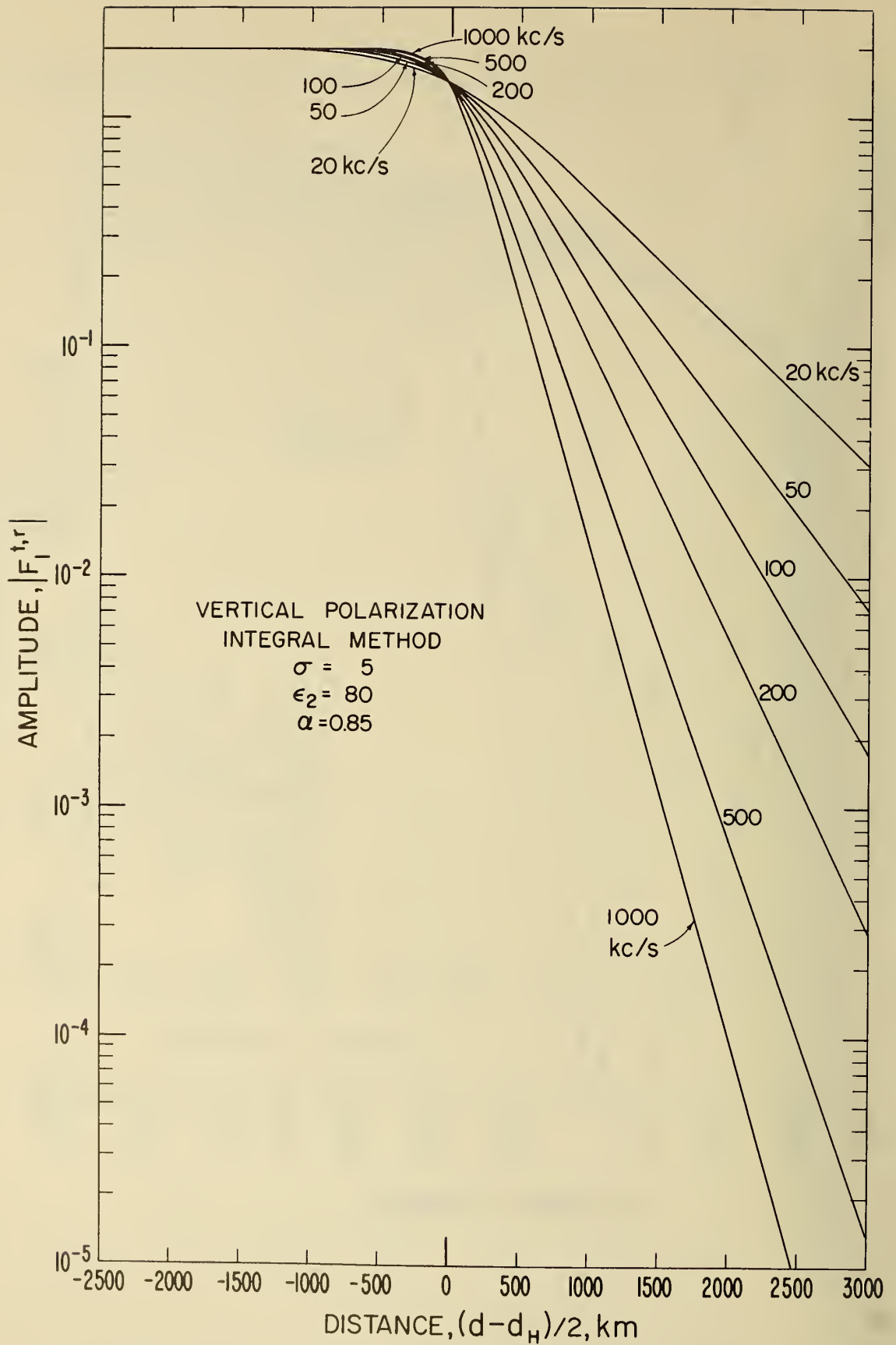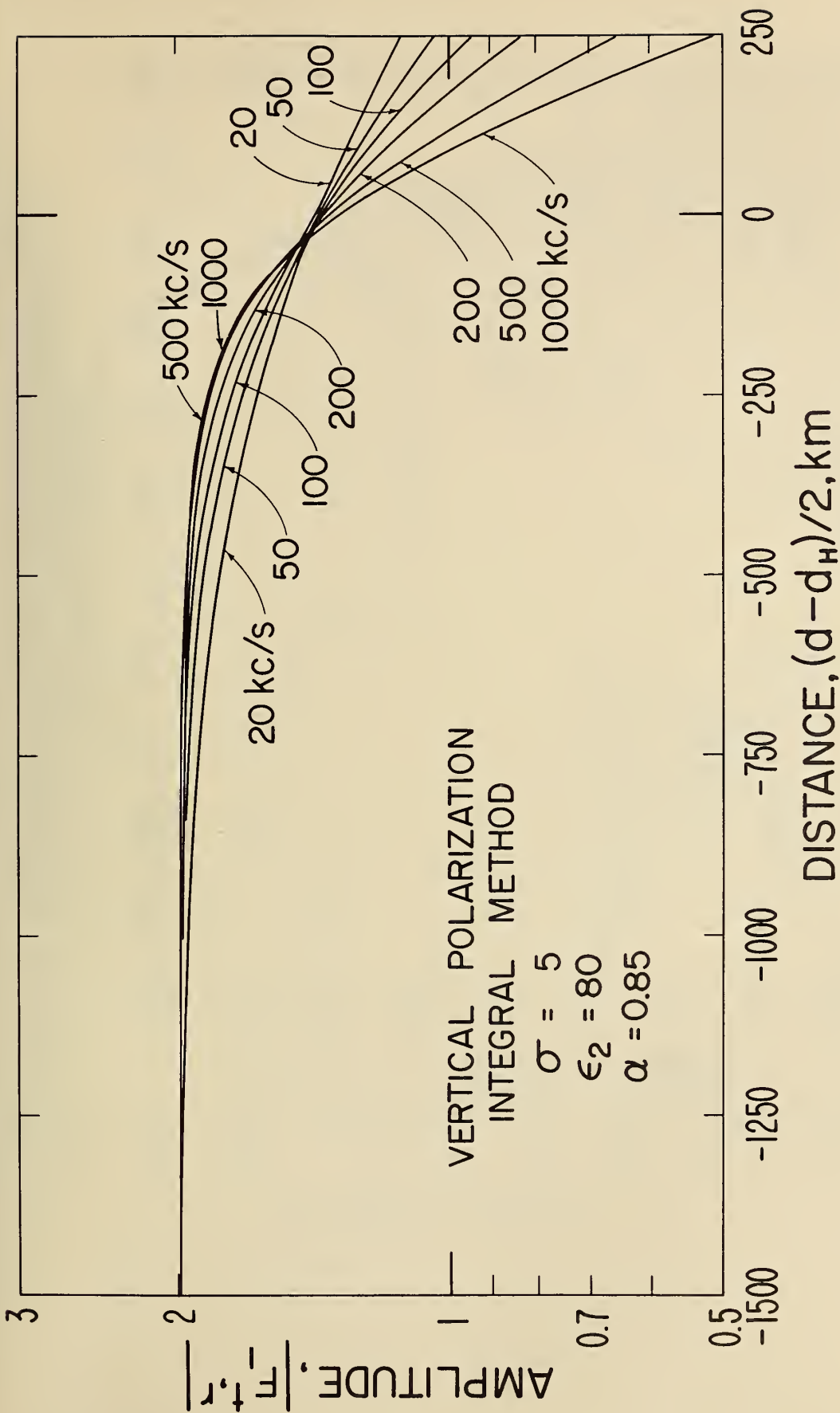
Figure 6. Amplitude of the cut-back factor $F_1^{t,r}$.
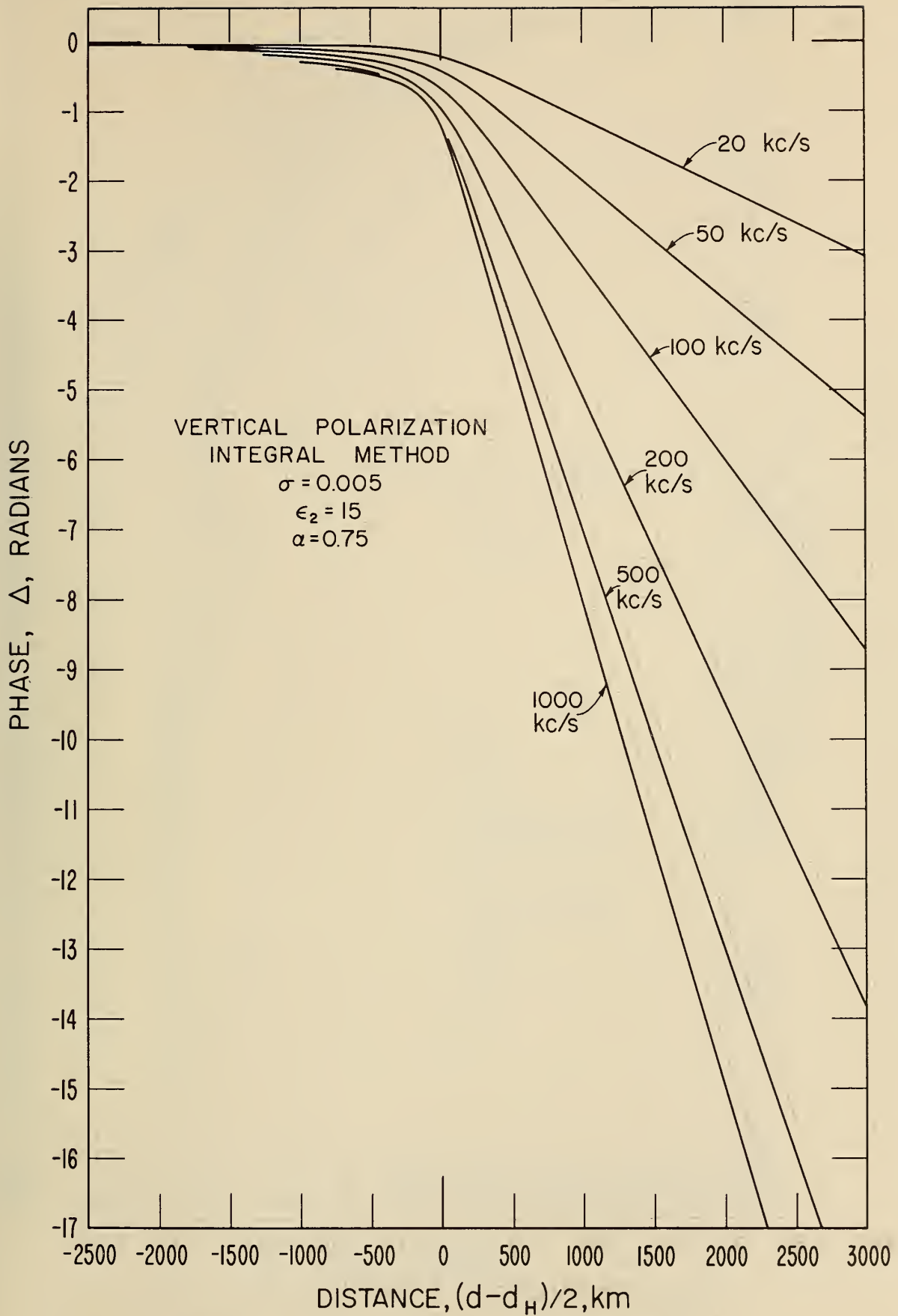
Figure 7.   Phase of the cut-back factor $F_1^t{}'^r$.

-17-
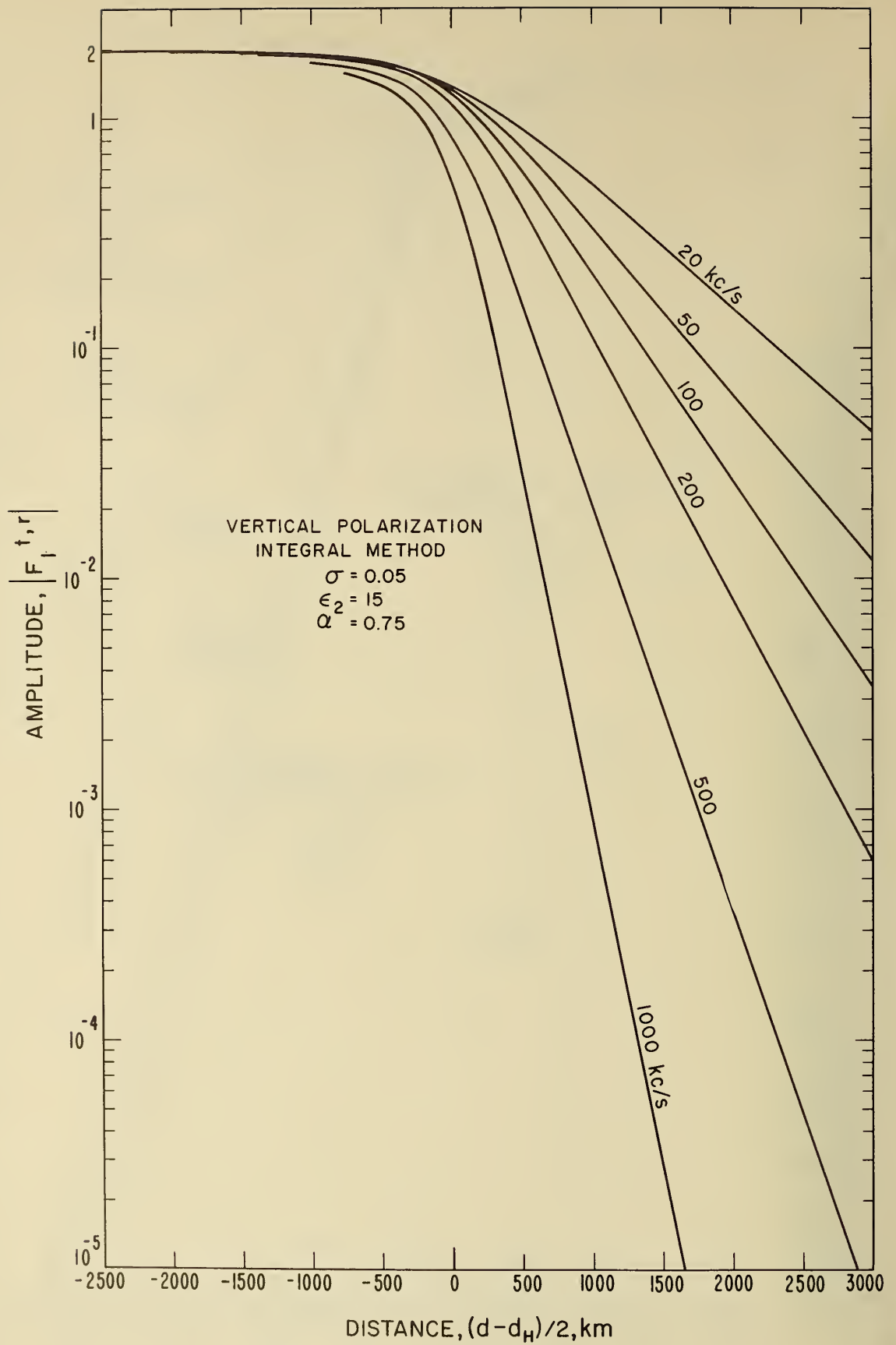
Figure 8. Amplitude of the cut-back factor $F_1^{t,\,r}$.
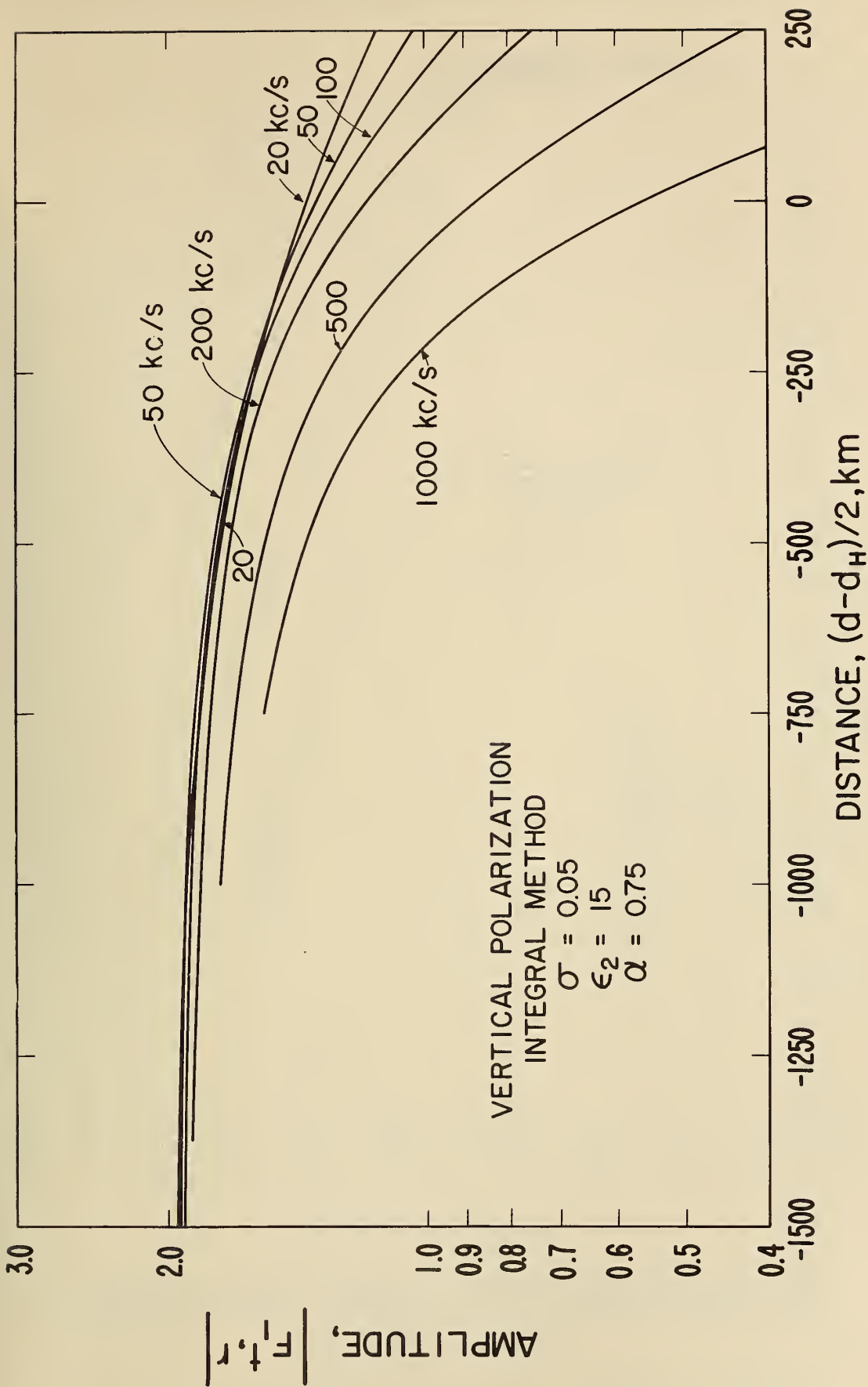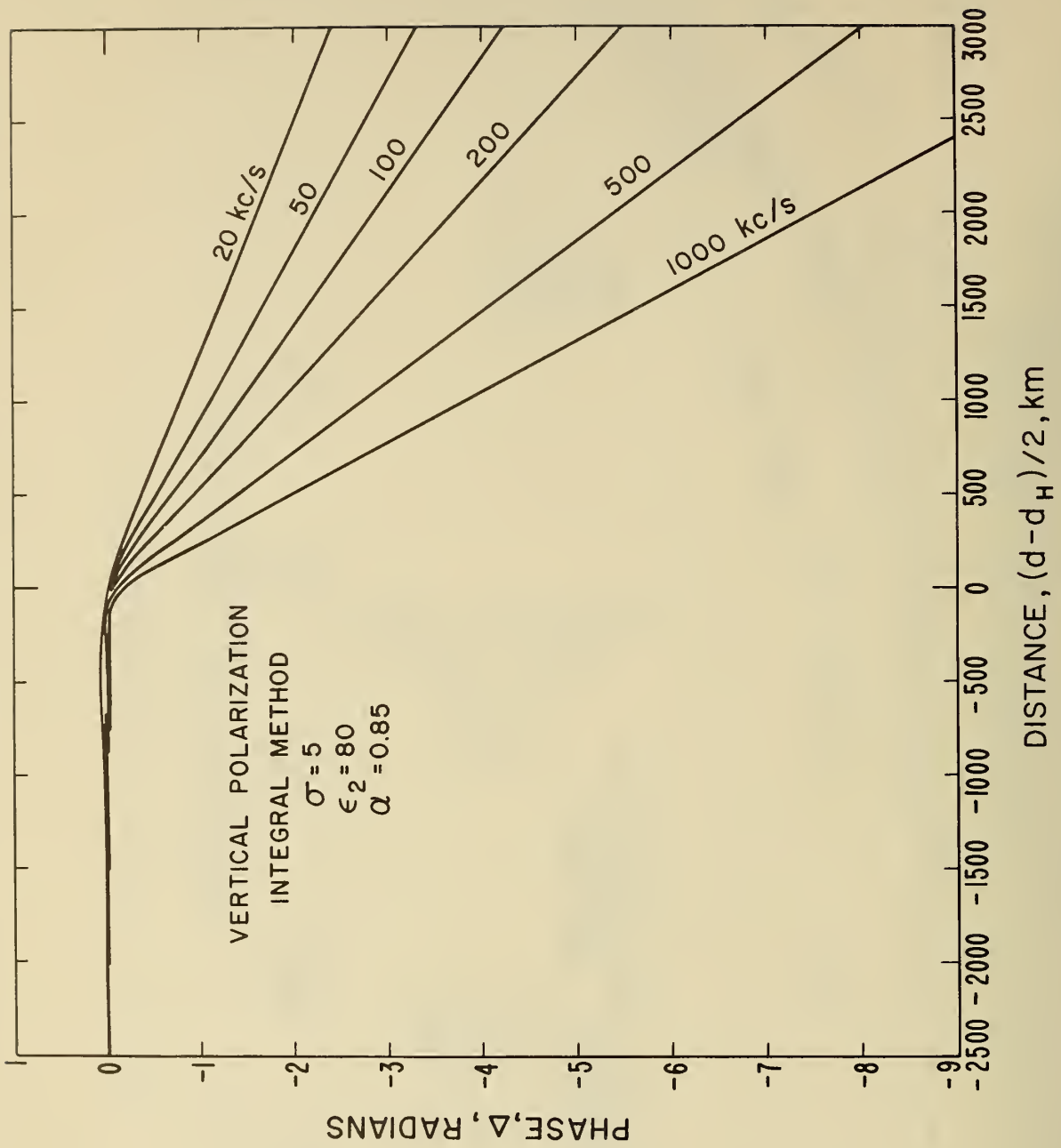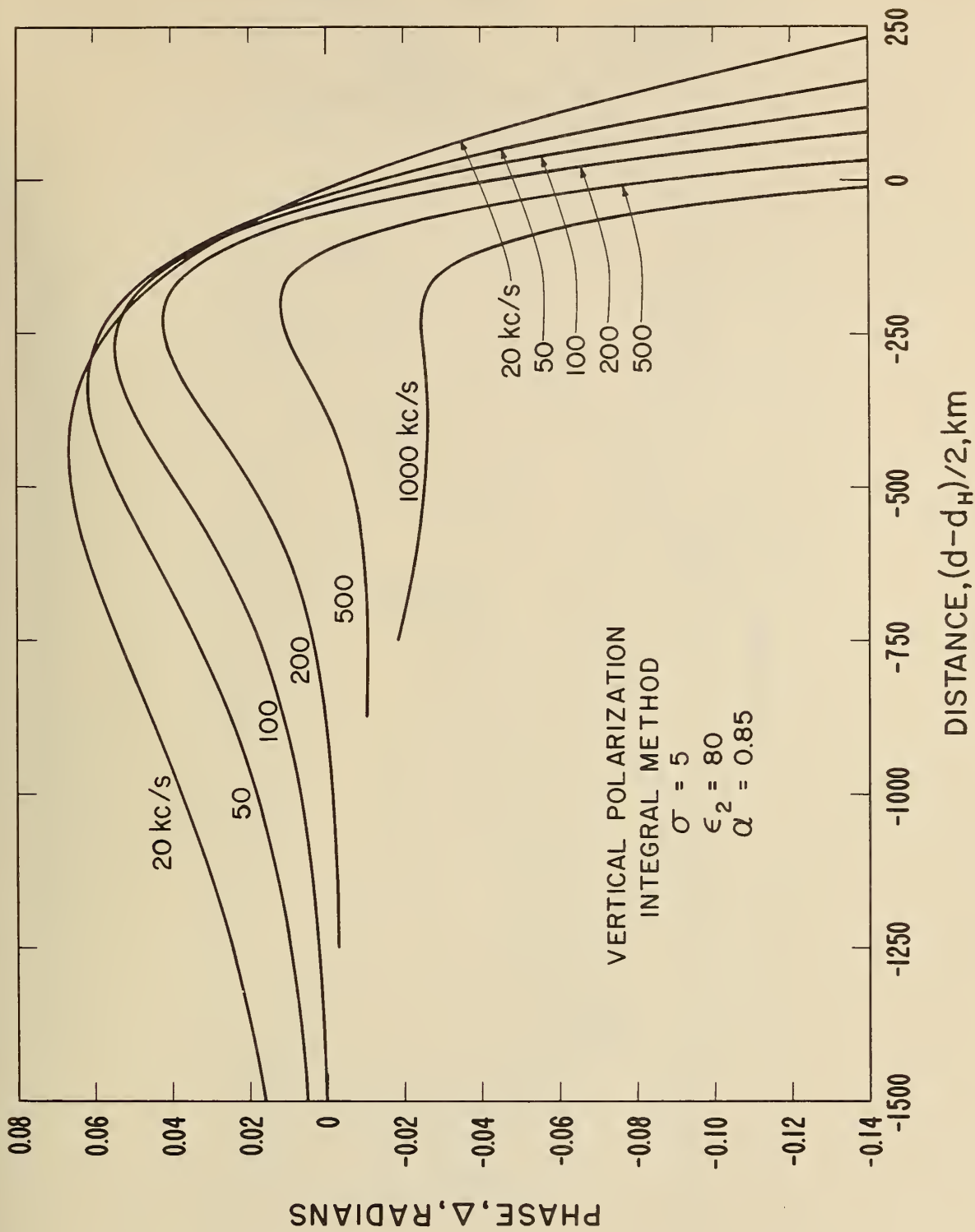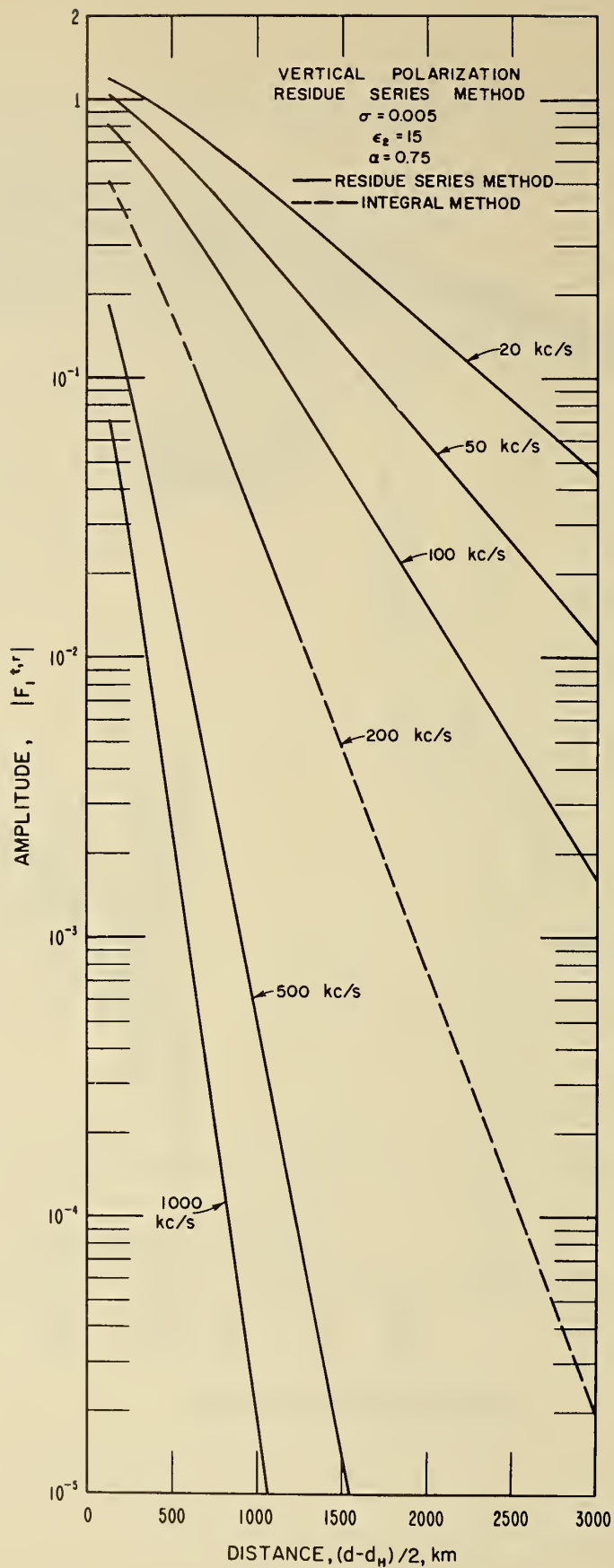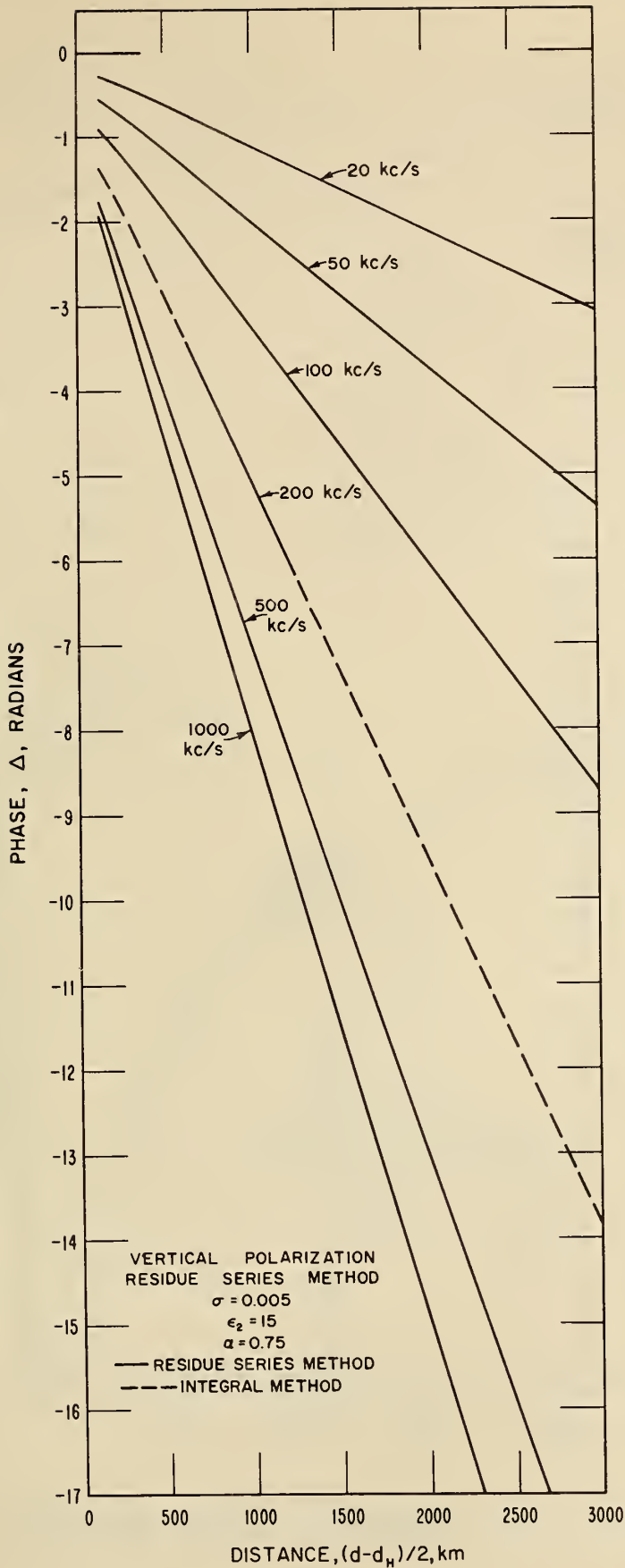
Figure 9. Amplitude of the cut-back factor $F_1^{t',r}$.
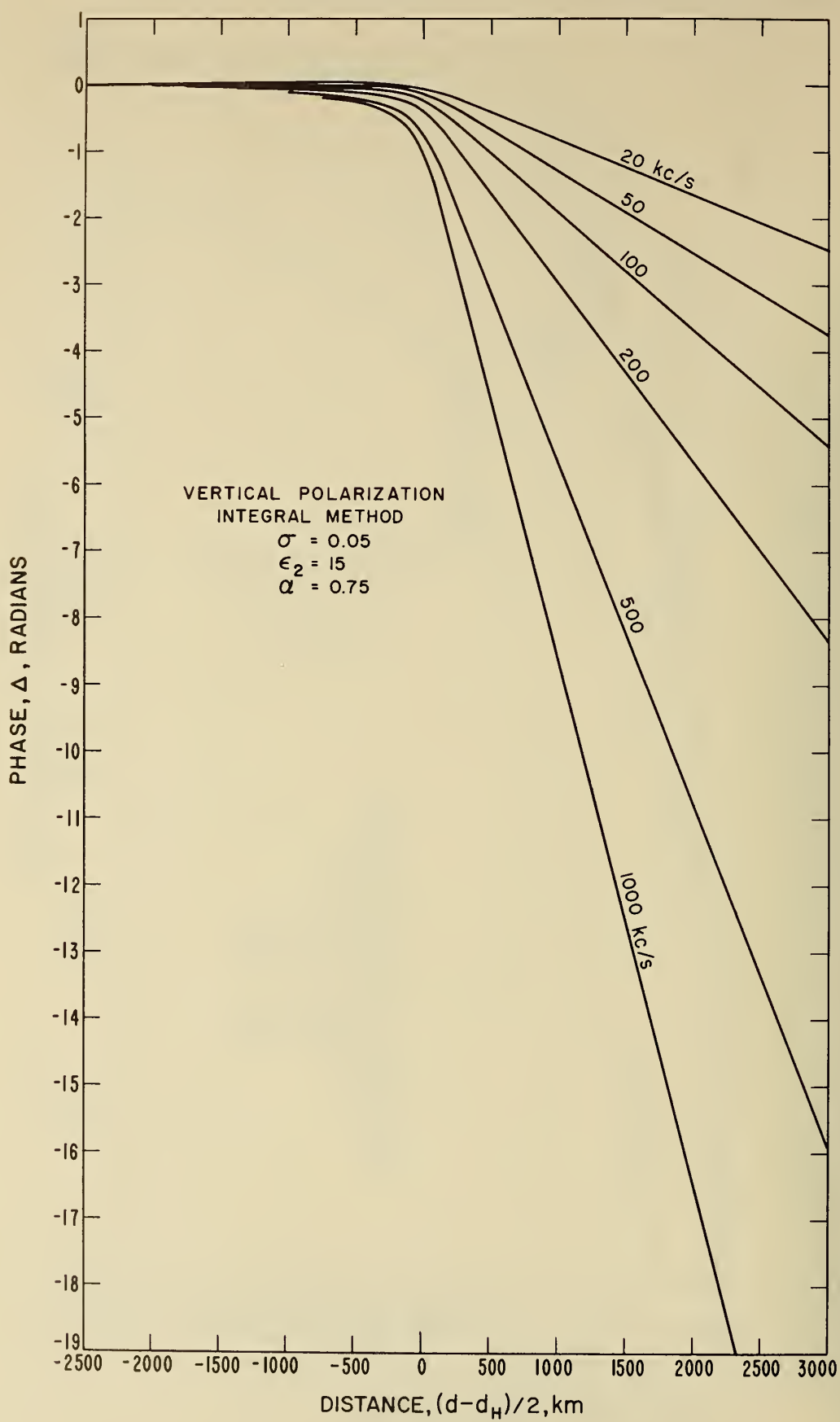
Figure 10. Phase of the cut-back factor $F_1^{t,r}$.
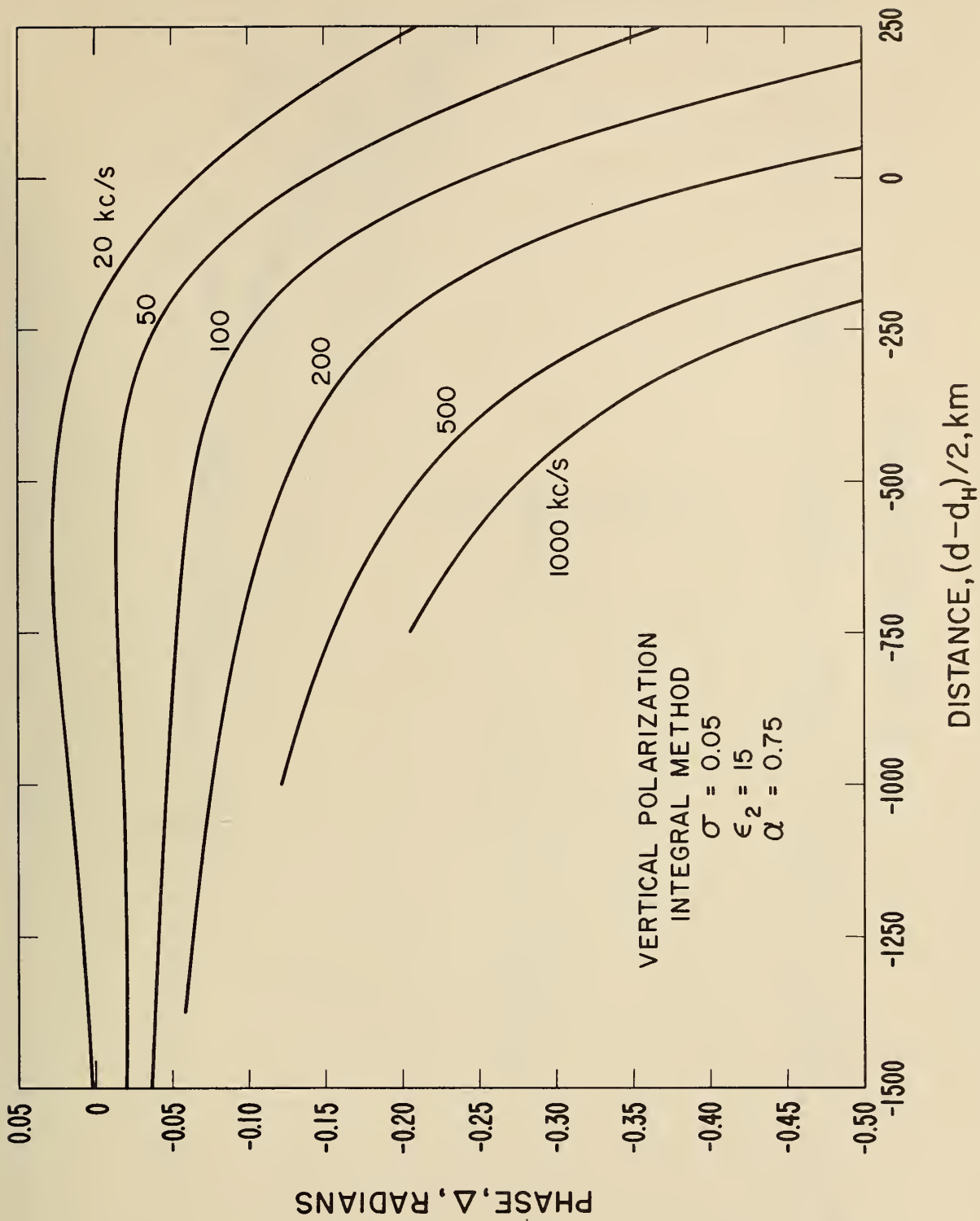
Figure 11. Phase of the cut-back factor $F_1^{t,r}$.

VERTICAL POLARIZATION
INTEGRAL METHOD
$\sigma = 0.05$
$\epsilon_2 = 15$
$\alpha^2 = 0.75$

20 kc/s
50
100
200
500
1000 kc/s

DISTANCE, $(d-d_H)/2$, km

PHASE, Δ, RADIANS

-21-
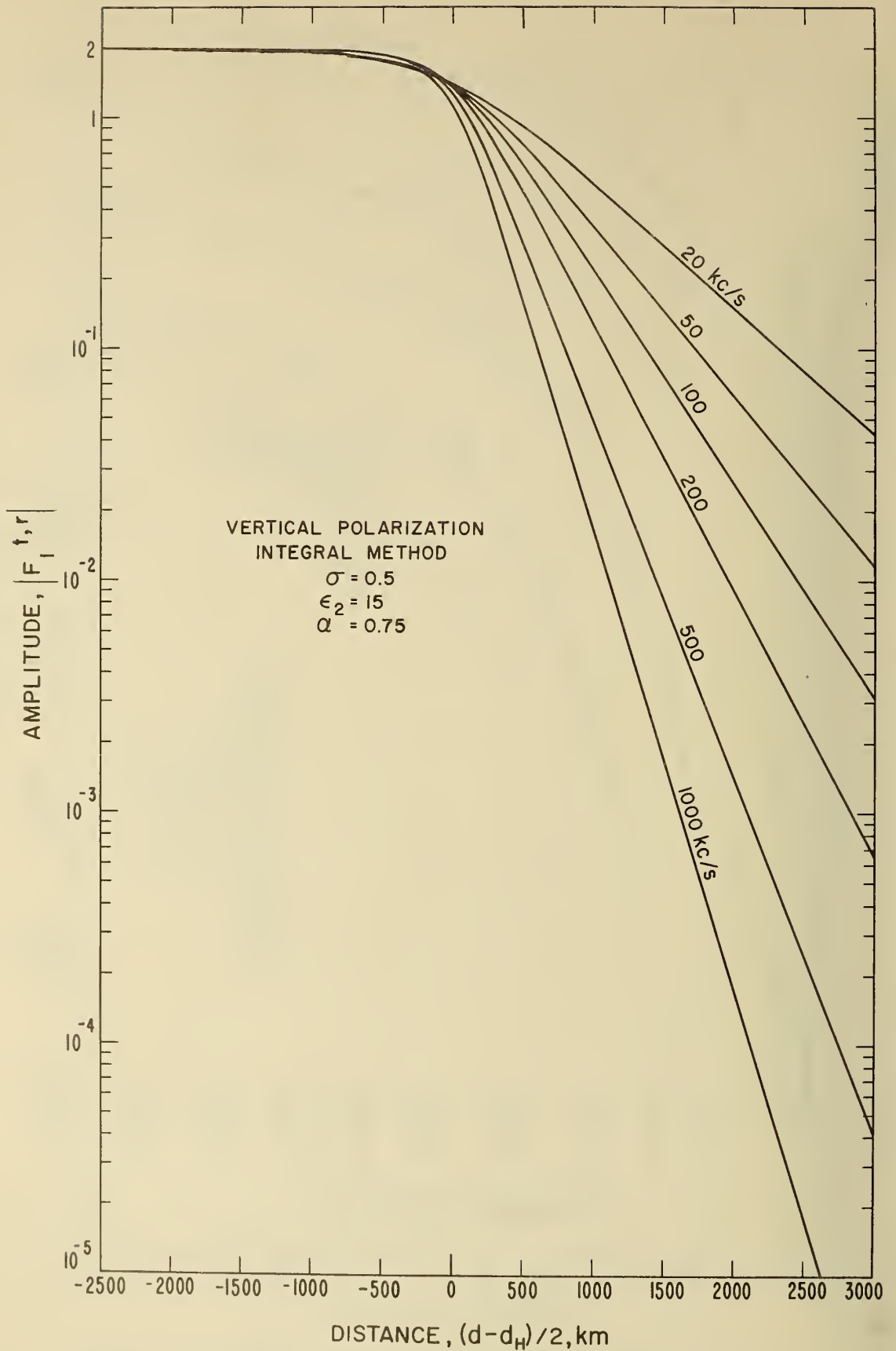
Figure 12.　Amplitude of the cut-back factor $F_1^{t,r}$.
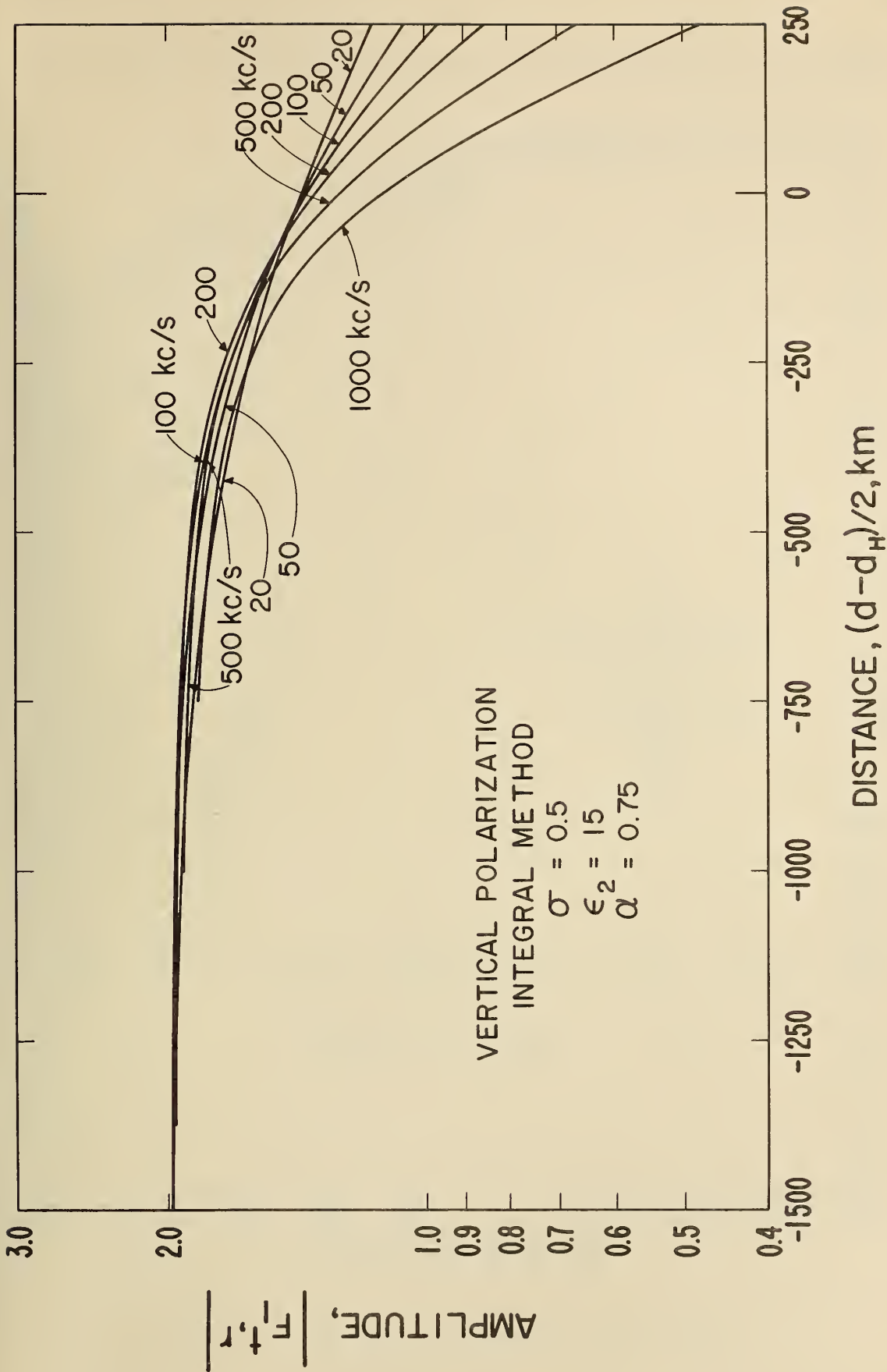
Figure 13. Amplitude of the cut-back factor $F_1^{t,r}$.
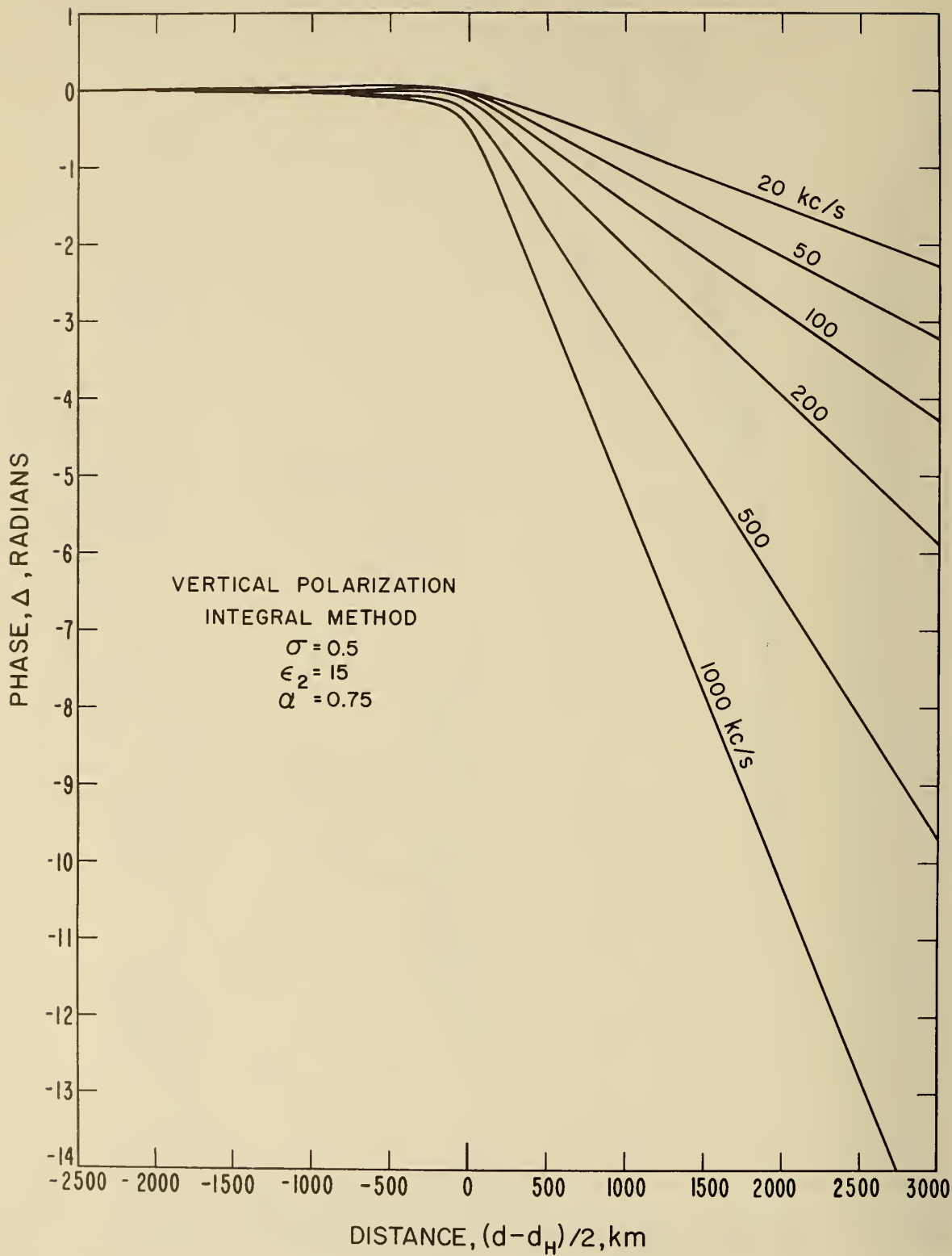
Figure 14. Phase of the cut-back factor $F_1^{t,r}$.
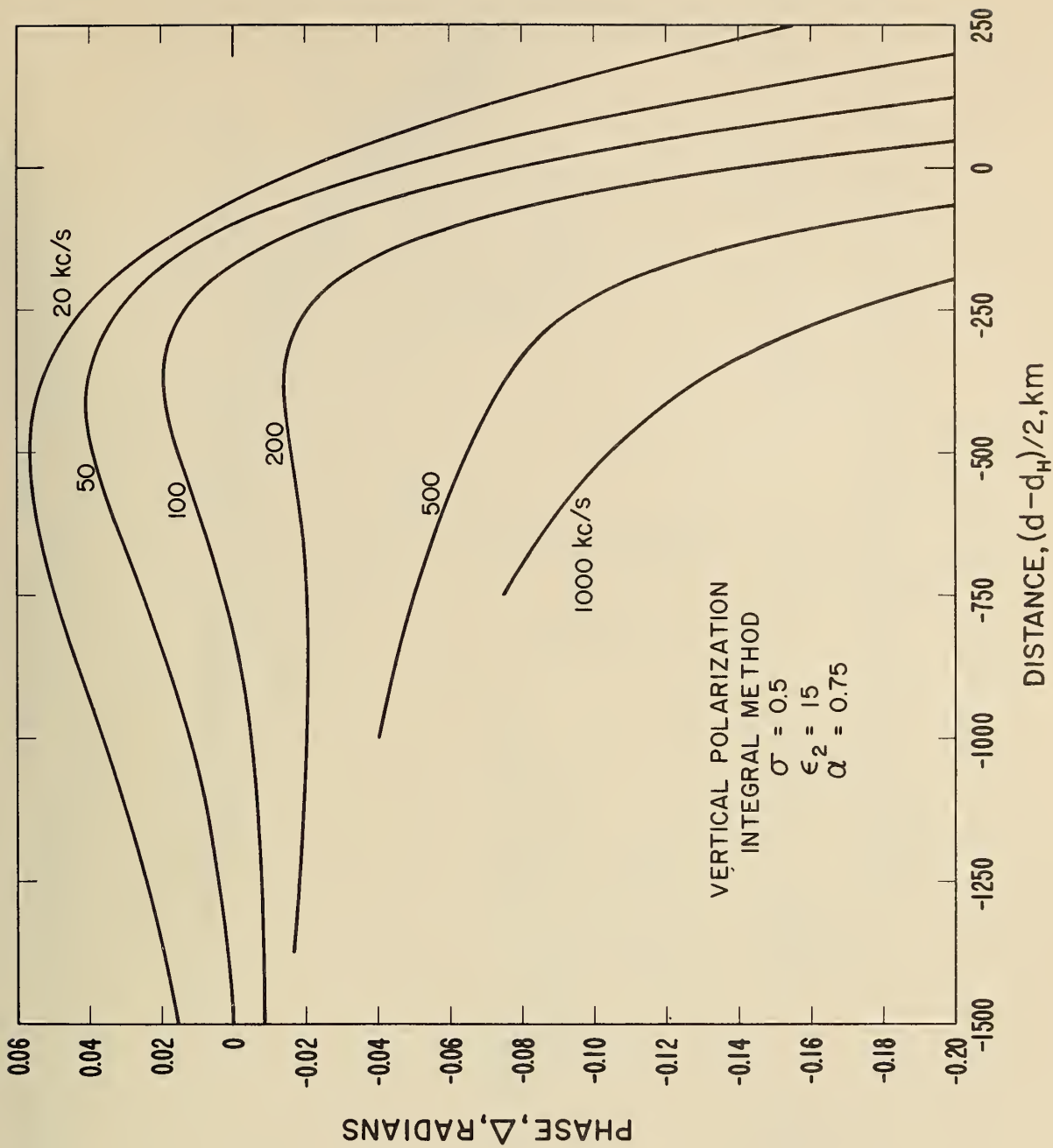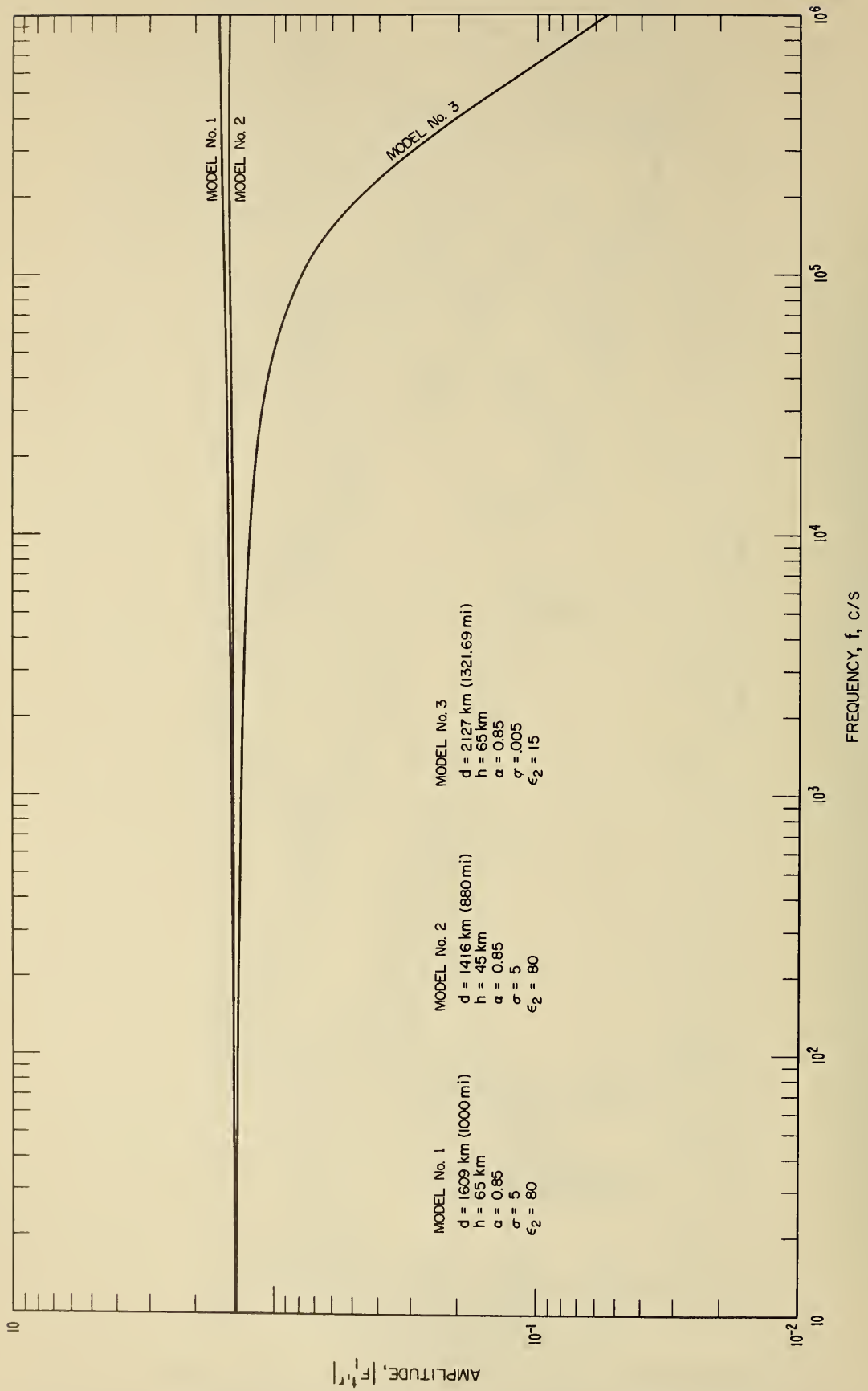
Figure 15. Phase of the cut-back factor $F_1^{t,r}$.

Figure 16. Amplitude of the cut-back factor $F_1^{t,r}$.

-26-

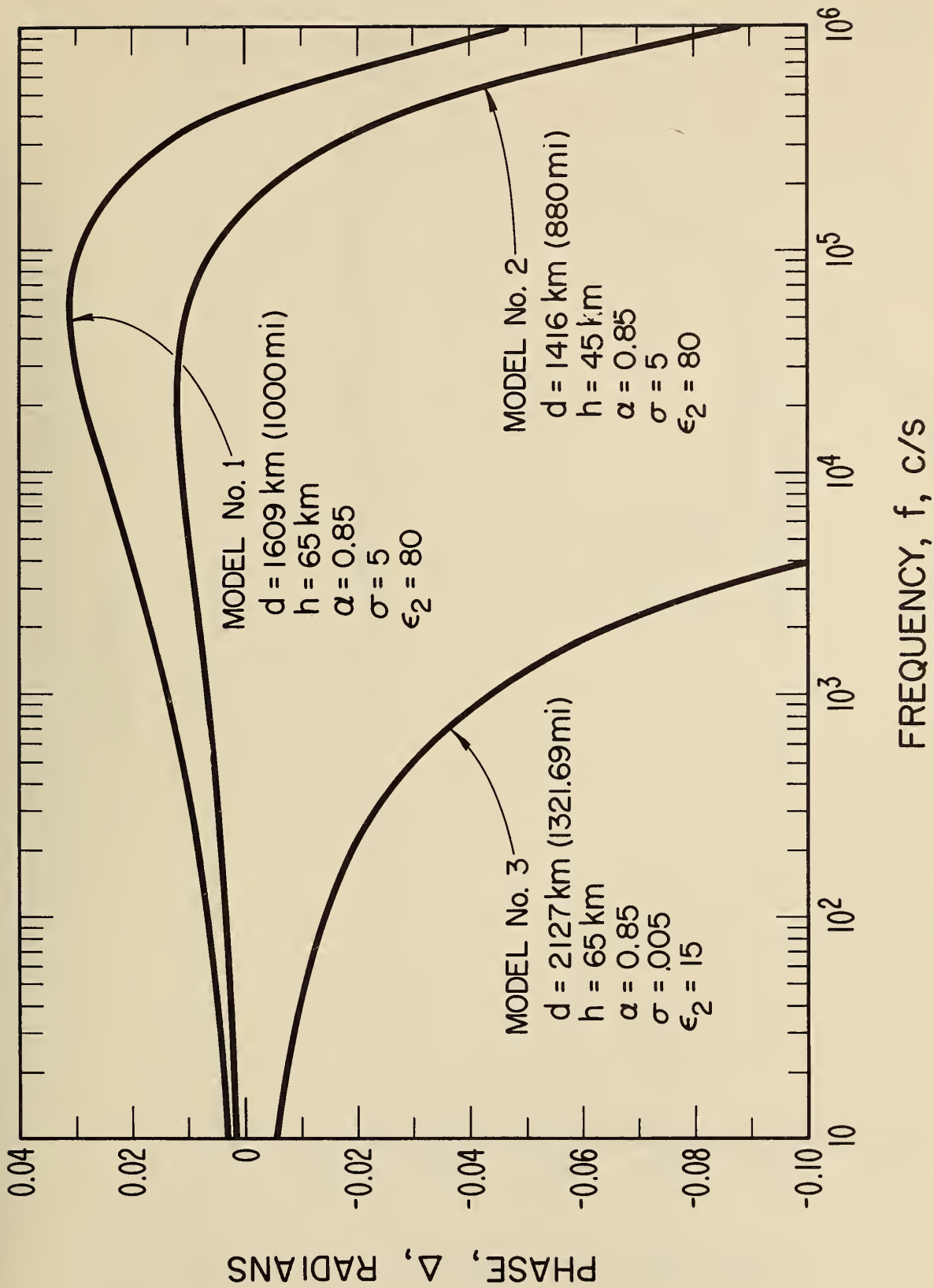Figure 17. Amplitude of the cut-back factor $F_1^{t',r}$.

Figure 18. Phase of the cut-back factor $F_1^{t,r}$.

Figure 19. Phase of the cut-back factor $F_1^{t,r}$.

Figure 20.   Amplitude of the cut-back factor $F_1^{t,r}$.

Figure 21. Amplitude of the cut-back factor $F_1^{t,r}$.

Figure 22.   Phase of the cut-back factor $F_1^{t, r}$.

Figure 23. Phase of the cut-back factor $F_1^{t,r}$.

Figure 24.   Amplitude of the cut-back factor $F_1^{t,r}$.

Figure 25.   Phase of the cut-back factor $F_1^{t,r}$.

Figure 26.   Amplitude of the cut-back factor $F_1^{t''}$.

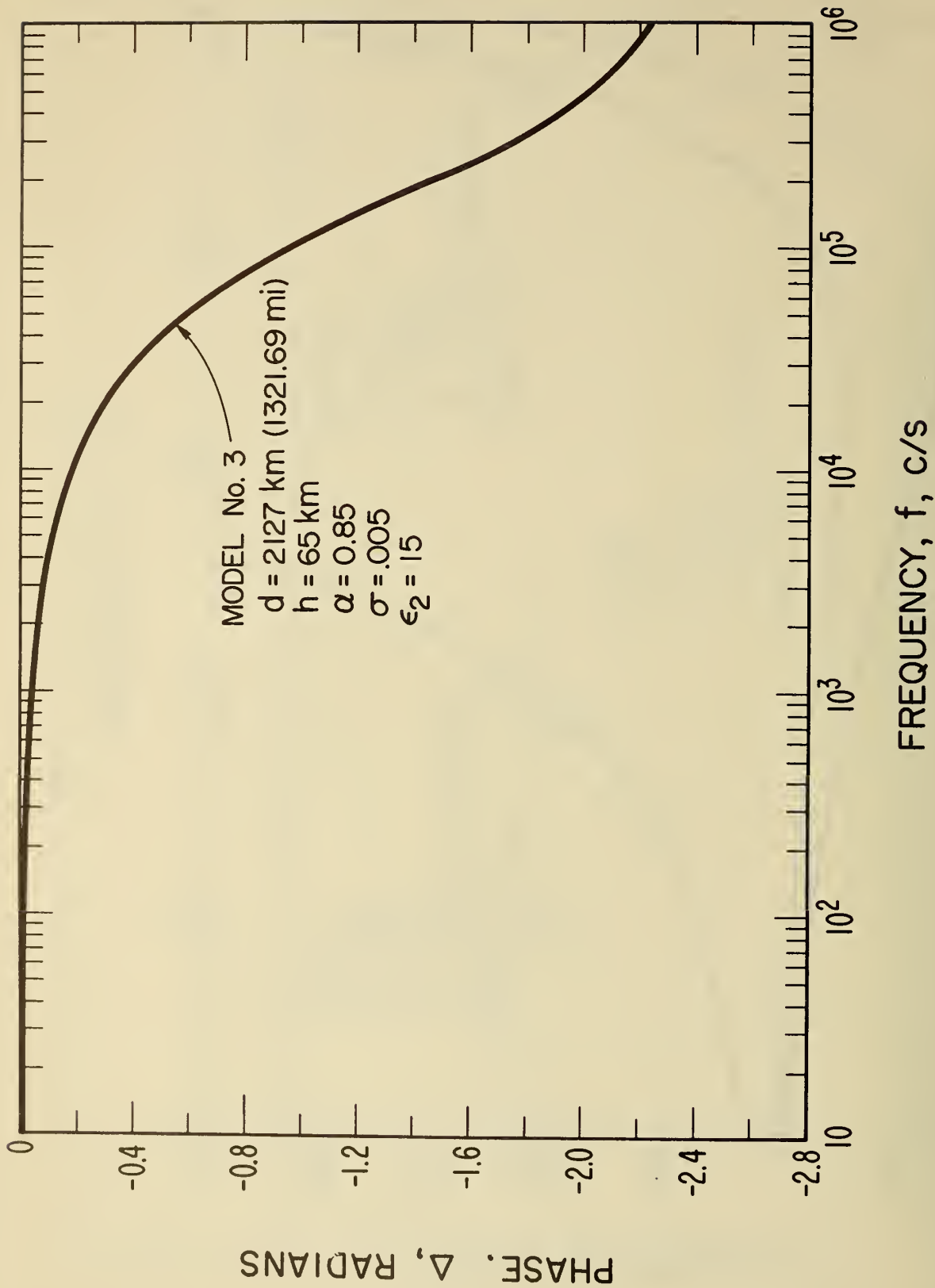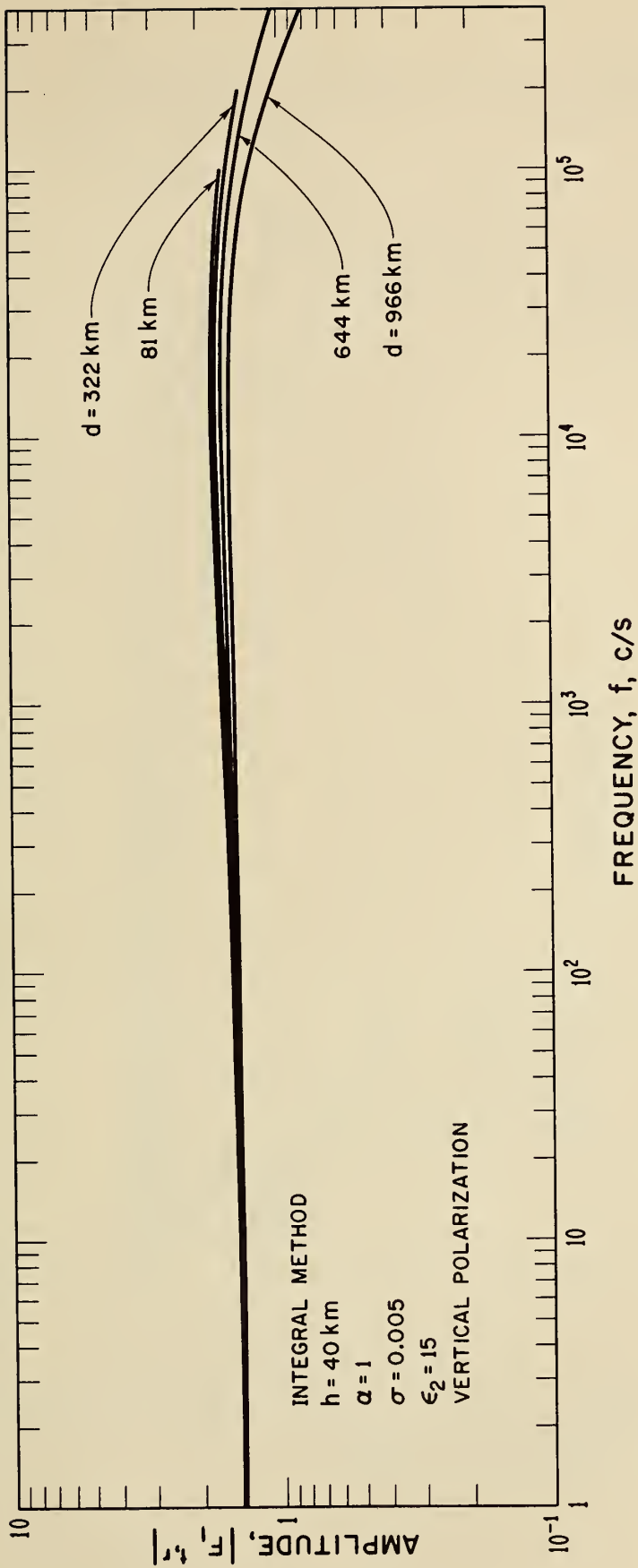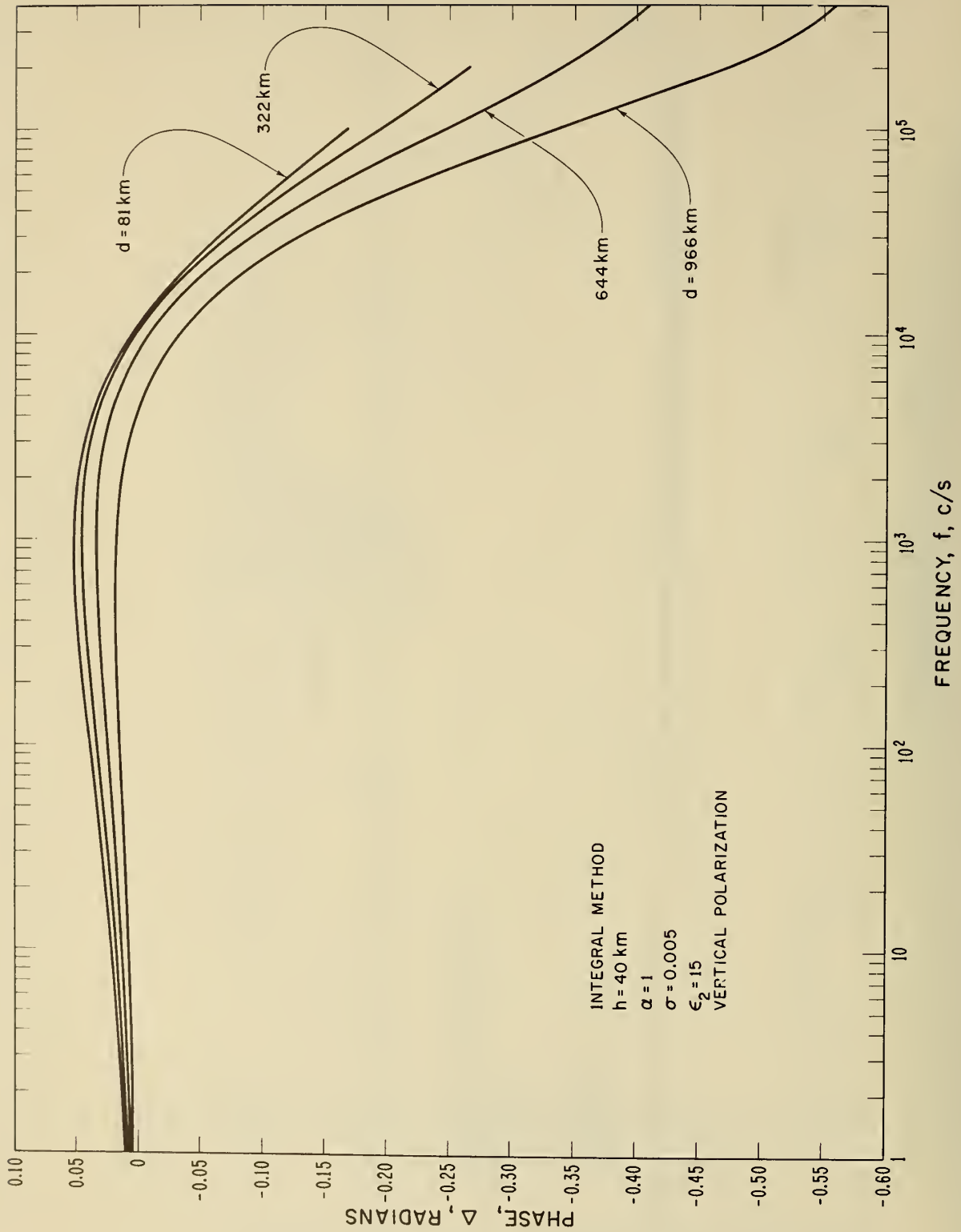Figure 27. Phase of the cut-back factor F_1^t, r.

MODEL No. 3
d = 2127 km (1321.69 mi)
h = 65 km
α = 0.85
σ = .005
ϵ_2 = 15

FREQUENCY, f, c/s

PHASE, Δ, RADIANS

Figure 28.   Phase of the cut-back factor $F_1^{t,r}$.

Figure 29. Amplitude of the cut-back factor $F_1^{t, r}$.
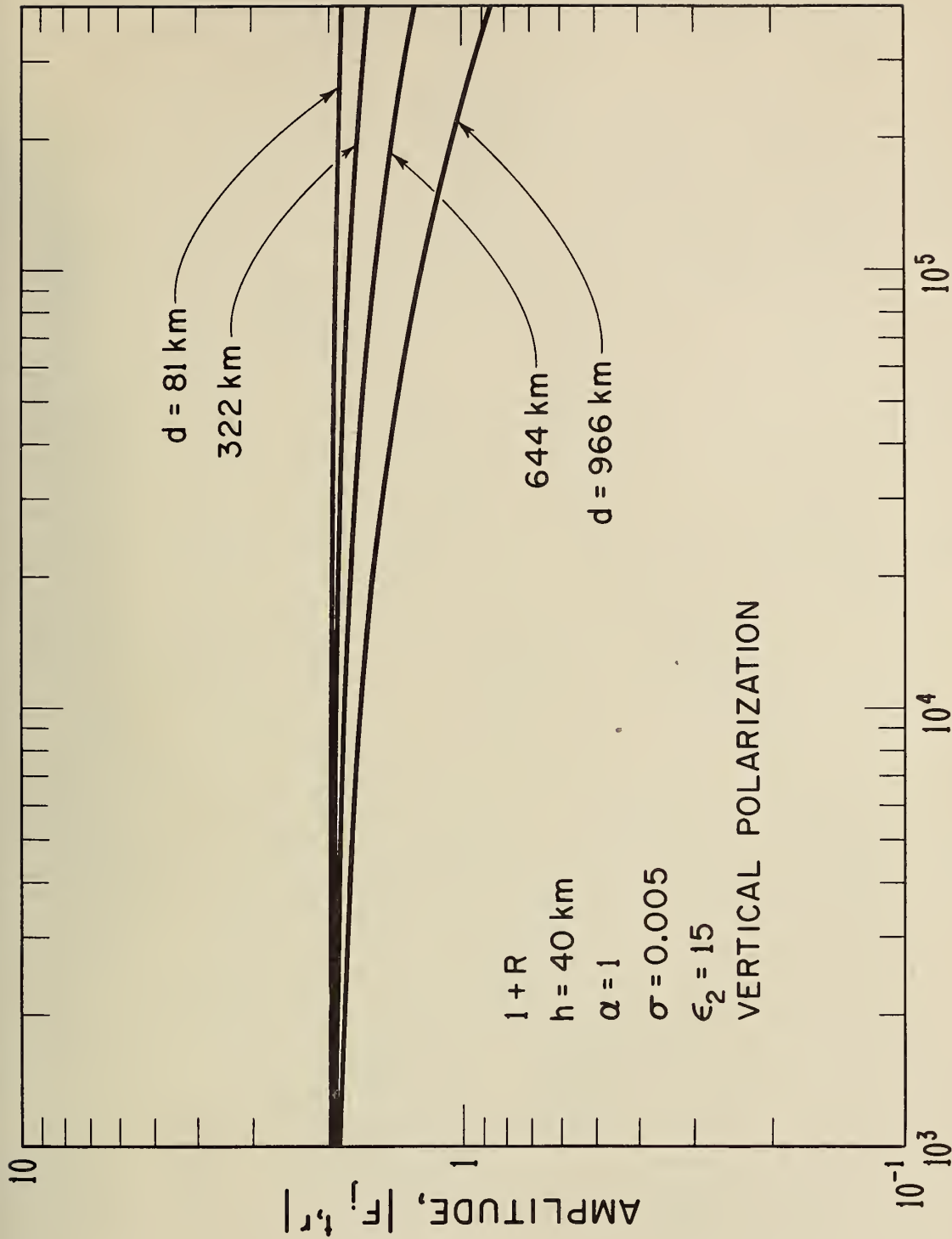
-39-

Figure 30. Phase of the cut-back factor $F_1^{t,r}$.

INTEGRAL METHOD
h = 40 km
$\alpha = 1$
$\sigma = 0.005$
$\epsilon_2 = 15$
VERTICAL POLARIZATION

FREQUENCY, f, c/s

PHASE, Δ, RADIANS

Figure 31. Amplitude of the cut-back factor $F_j^{t,r}$.
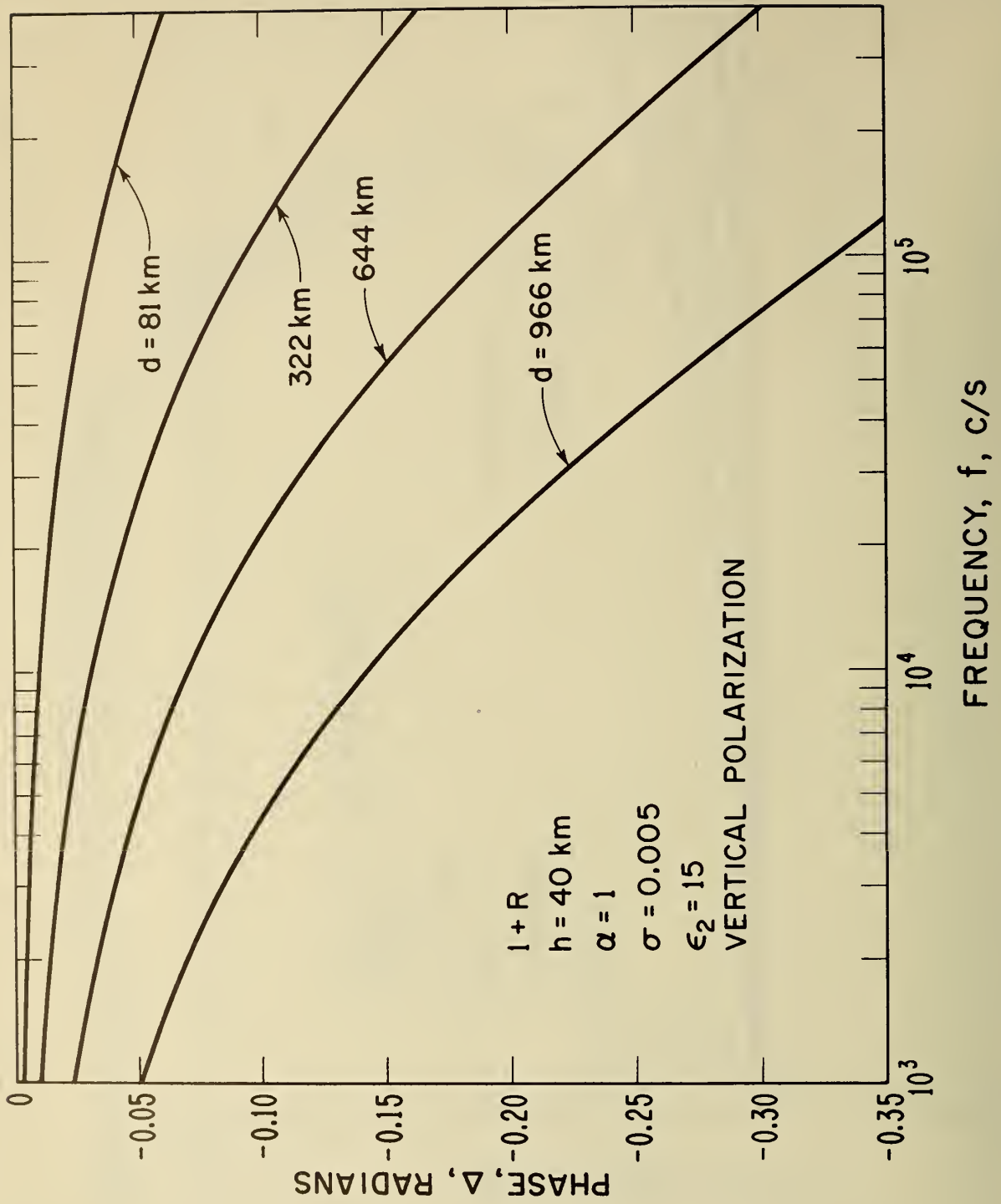
Figure 32.   Phase of the cut-back factor $F_j^{t,r}$.